© 2016. Published by The Company of Biologists Ltd | Development (2016) 143, 2767-2779 doi:10.1242/dev.132746

RESEARCH ARTICLE

The methyltransferase *Setdb1* is essential for meiosis and mitosis in mouse oocytes and early embryos

Angeline Eymery[1], Zichuan Liu[1,*], Evgeniy A. Ozonov[1,*], Michael B. Stadler[1,2] and Antoine H. F. M. Peters[1,3,‡]

ABSTRACT

Oocytes develop the competence for meiosis and early embryogenesis during their growth. Setdb1 is a histone H3 lysine 9 (H3K9) methyltransferase required for post-implantation development and has been implicated in the transcriptional silencing of genes and endogenous retroviral elements (ERVs). To address its role in oogenesis and pre-implantation development, we conditionally deleted *Setdb1* in growing oocytes. Loss of *Setdb1* expression greatly impaired meiosis. It delayed meiotic resumption, altered the dynamics of chromatin condensation, and impaired kinetochore-spindle interactions, bipolar spindle organization and chromosome segregation in more mature oocytes. The observed phenotypes related to changes in abundance of specific transcripts in mutant oocytes. *Setdb1* maternally deficient embryos arrested during pre-implantation development and showed comparable defects during cell cycle progression and in chromosome segregation. Finally, transcriptional profiling data indicate that *Setdb1* downregulates rather than silences expression of ERVK and ERVL-MaLR retrotransposons and associated chimearic transcripts during oogenesis. Our results identify *Setdb1* as a newly discovered meiotic and embryonic competence factor safeguarding genome integrity at the onset of life.

KEY WORDS: Histone methylation, Meiosis, Mitosis, Pre-implantation development, Transcriptional regulation

INTRODUCTION

Mouse female germ cells enter meiosis during fetal development and arrest at the dictyate stage of meiotic prophase I shortly after birth until adulthood. During folliculogenesis, arrested oocytes grow in size and accumulate many transcripts and proteins, conferring the ability to progress through meiosis (meiotic competence) and to support early embryonic development (developmental competence) in absence of transcription (Hirao et al., 1993; Inoue et al., 2008; Wickramasinghe et al., 1991; Zuccotti et al., 2011, 2002).

In fully grown oocytes, also called germinal vesicle (GV) oocytes, chromatin undergoes an extensive remodeling, changing from a so-called non-surrounded nucleolus (NSN) to a surrounded nucleolus (SN) configuration, which normally coincides with a global shutdown of transcription (Bouniol-Baly et al., 1999; De La Fuente, 2006; Liu and Aoki, 2002; Moore et al., 1974). Meiotic arrest in GV oocytes is maintained by high levels of the 'second messenger' cyclic adenosine monophosphate (cAMP), which activates protein kinase A (PKA) to phosphorylate downstream-acting proteins, which in turn suppress activity of the so-called maturation promoting factor (MPF). MPF, consisting of Cdk1 and cyclin B, is the major driver of meiotic resumption (Dekel, 1996; Grieco et al., 1996; Han and Conti, 2006; Schultz et al., 1983). Meiotic resumption is triggered by a surge of the luteinizing hormone (LH), which activates the phosphodiesterase Pde3A to hydrolyze cAMP and to drive entry into meiotic maturation (Sun et al., 2009) as reflected, for example, by the breakdown of the nuclear envelope (also called GV breakdown, or GVBD). Alterations of this pathway often lead to infertility as exemplified by the arrest of oocytes at the GV stage in absence of *Pde3a* (Beall et al., 2010; Masciarelli et al., 2004). Following GVBD, oocytes condense their chromatin, align chromosomes on the metaphase I (MI) plate by a functional spindle, undergo chromosome segregation and extrude the first polar body (PB), to ultimately become arrested at metaphase II (MII). Spindle assembly in oocytes is driven by acentriolar centrosomes, called MTOCs (microtubule organization centers) that cluster together to form a bipolar spindle (Schuh and Ellenberg, 2007). Interactions between microtubules and kinetochores on chromosomes ensure proper chromosome segregation (Watanabe, 2012). Following fertilization, embryonic cleavage divisions share initially common mechanisms with meiosis such as a cAMP-PKA-dependent nuclear envelope breakdown (NEBD) and MTOC-driven bipolar spindle formation (Courtois et al., 2012; Cui et al., 2008; Poueymirou and Schultz, 1987; Yu et al., 2008). The organization of spindles gradually transitions over eight cleavage divisions from a large meiotic spindle into a short mitotic spindle harboring centrosomes (Courtois et al., 2012; Kubiak et al., 2008).

In mammals, several H3K9 methyltransferases suppress gene transcription and restrict differentiation potential during development (Nestorov et al., 2013; Shi et al., 2008). Setdb1 is able to mono-, di- and tri-methylate H3K9 (Loyola et al., 2009; Wang et al., 2003). *Setdb1* is essential for pluripotency maintenance and repression of trophectodermal differentiation in embryonic stem cells (ESCs) (Lohmann et al., 2010; Yeap et al., 2009; Yuan et al., 2009), and for primordial germ cell (PGC) and neuronal progenitor development (Tan et al., 2012). Moreover, in these cells *Setdb1* is required for H3K9me3 deposition at and transcriptional silencing of endogenous long terminal repeat (LTR)-containing retroviruses (ERVs) such as those belonging to the ERV1 (class I) and ERVK [class II; including intracisternal A-type particle (IAP) and early transposons (ETn/MusD)] repeat families. In contrast, ERVs belonging to class III families [ERVL elements (muERV-L/MERVL) and mammalian apparent LTR retrotransposons (ERVL-MaLR)] as well as non-LTR retrotransposons like long interspersed nuclear elements (LINEs) and short interspersed nuclear elements

[1]Friedrich Miescher Institute for Biomedical Research, Basel 4058, Switzerland. [2]Swiss Institute of Bioinformatics, Basel 4058, Switzerland. [3]Faculty of Sciences, University of Basel, Basel 4056, Switzerland.
*These authors contributed equally to this work

‡Author for correspondence (antoine.peters@fmi.ch)

A.H.F.M.P., 0000-0002-0311-1887

Received 11 November 2015; Accepted 2 June 2016

Development (2016) 143, 2767-2779 doi:10.1242/dev.132746

(SINEs) remained repressed (Karimi et al., 2011; Liu et al., 2014; Matsui et al., 2010; Tan et al., 2012). *Setdb1*-mediated repression of ERVs is required to prevent ERV-driven expression of nearby genes (Karimi et al., 2011; Tan et al., 2012).

In mouse oocytes and early pre-implantation embryos, however, many LTR and non-LTR retrotransposons are expressed. In oocytes, predominantly ERVL-MaLRs and, to a lesser extent, ERVK retrotransposons are transcribed. These elements also control gene expression through formation of chimeric transcripts (Fadloun et al., 2013; Peaston et al., 2004; Svoboda et al., 2004; Veselovska et al., 2015). In early embryos, ERVL, ERVK and ERV1 retrotransposons, as well as LINEs, are more highly expressed than ERVL-MaLRs (Fadloun et al., 2013; Ribet et al., 2008).

Setdb1 is essential for early development as mutant embryos die shortly after implantation (Dodge et al., 2004). It is highly expressed during oogenesis and is maternally provided to the embryo. Interestingly, *Setdb1* is embryonically not transcribed prior to the blastocyst stage (Cho et al., 2011; Dodge et al., 2004). Maternal Setdb1 protein might therefore contribute to meiotic maturation and pre-implantation embryogenesis. Here, we address the function of Setdb1 for these processes by deleting *Setdb1* in growing oocytes. We observed aberrant PKA signaling in mature *Setdb1* mutant oocytes and a delay in meiotic resumption. In addition, kinetochore-spindle interactions, bipolar spindle organization and chromosome segregation are defective in $Setdb1^{-/-}$ oocytes. These phenotypic defects relate to changes in gene expression measured in $Setdb1^{-/-}$ oocytes. Maternal *Setdb1* expression is also crucial for embryonic development as cell cycle progression and chromosome segregation are similarly impaired in maternally deficient embryos. We further measured upregulation of ERVL-MaLR and ERVK retrotransposons and an increase in frequency of splice junctions between these ERVs and gene exons in $Setdb1^{-/-}$ oocytes. This study identifies *Setdb1* as a maternal transcriptional co-regulator of genes implicated in cell cycle progression and chromosome segregation in oocytes and early embryos, and as a modulator of ERV repression.

RESULTS

Loss of maternal *Setdb1* impairs early embryonic development

To investigate the function of maternally provided *Setdb1* in early embryogenesis, we deleted *Setdb1* in growing oocytes and analyzed embryonic development of offspring. We generated animals that carried floxed alleles of *Setdb1* ($Setdb1^{f/f}$) (Fig. S1A) and a transgenic allele of *Cre* recombinase that is specifically expressed in growing oocytes under the control of the *Zona pellucida 3* promoter (*Zp3*-cre). By crossing *Setdb1* mutant ($Setdb1^{f/f}$;*Zp3*-cre) females with *Setdb1* floxed ($Setdb1^{f/f}$) control males we did not obtain any offspring, whereas crosses with $Setdb1^{f/f}$ or heterozygous ($Setdb1^{f/+}$;*Zp3*-cre) control females produced offspring (Fig. 1A). To investigate when embryonic lethality occurred, we flushed embryos at day 3.5 of their development (E3.5) from the uteri of control and mutant females (Fig. 1B). Though many embryos from a $Setdb1^{f/f}$ intercross had developed to the blastocyst stage, all embryos from *Setdb1* mutant females and $Setdb1^{f/f}$ males, being deficient for maternal (m−) but wild type for zygotic (z+) expression, died before the blastocyst stage (Fig. 1B; Fig. S1B).

To analyze in more detail the impairment of pre-implantation development we isolated zygotes and cultured them for 3 days *in vitro*. The development of $Setdb1^{m-z+}$ embryos was progressively delayed compared with that of control embryos (Fig. 1C,D). None of the $Setdb1^{m-z+}$ embryos developed into blastocysts, even when cultured for an additional day (Fig. S1C). Together, these results demonstrate that maternally provided *Setdb1* is essential for pre-implantation development.

Loss of *Setdb1* does not affect folliculogenesis but reduces global H3K9me2 levels in oocytes

As *Setdb1* deletion occurred during oogenesis, embryonic arrest of $Setdb1^{m-z+}$ embryos could reflect defects occurring during oogenesis. Histological analysis revealed that the ovarian structure and folliculogenesis were unaltered in $Setdb1^{f/-}$;*Zp3*-cre females (Fig. 1E,F). Moreover, the average number of fully grown GV oocytes per mouse was similar between control and $Setdb1^{f/-}$;*Zp3*-cre females (Fig. 1G) and the percentages of immature NSN and mature SN GV oocytes were comparable (Fig. S1D), arguing that the genome-wide chromatin reorganization and condensation towards the GV stage is unaffected in $Setdb1^{-/-}$ oocytes. Together, these analyses did not reveal discernable differences in oocyte development in absence of *Setdb1*.

We next examined the levels of H3K9me1, H3K9me2 and H3K9me3 by immunofluorescence in GV oocytes (Fig. 1H,I). Setdb1 catalyzes mono-, di- and tri-methylation of H3K9 depending on interacting partners (Loyola et al., 2009; Wang et al., 2003). In $Setdb1^{-/-}$ oocytes, we observed reduced H3K9me2 levels. In contrast, H3K9me1 and H3K9me3 levels were unaltered. Given that *Setdb1* deficiency is induced in non-cycling oocytes, the differential effect on H3K9me1, H3K9me2 or H3K9me3 levels might reflect different degrees of modulation by histone demethylases, nucleosome turnover and/or compensatory re-methylation activities by other histone methyltransferases such as G9a (also known as Ehmt2), Glp1 (Ehmt1), Suv39h1 and Suv39h2. Indeed, we previously identified *Suv39h2* as a maternal regulator of H3K9me3 at constitutive heterochromatin (Puschendorf et al., 2008). Despite the reduction in the repressive H3K9me2 mark, the characteristic loss of chromatin association of RNA polymerase II (representative of global transcriptional shutdown) and the typical nuclear remodeling occurred properly in GV oocytes deficient for *Setdb1*, suggesting normal chromatin maturation in absence of *Setdb1* (Fig. S1E).

Loss of *Setdb1* impairs meiotic maturation

Meiotic maturation starts with GVBD of the oocyte, which is essential for female meiosis and prepares the oocyte for fertilization. We analyzed the efficiency of GVBD in control and $Setdb1^{-/-}$ oocytes at different time points after removal of milrinone, an inhibitor of the phosphodiesterase Pde3A and GVBD (see Fig. 6B), and observed that $Setdb1^{-/-}$ oocytes were delayed in undergoing GVBD. Moreover, more $Setdb1^{-/-}$ oocytes remained at the GV stage compared with control oocytes (Fig. 2A). We then studied in detail the process of meiotic maturation in oocytes that had undergone GVBD within 2 h or between 2 and 18 h after milrinone removal (‘early’ versus ‘late’ GVBD). We first determined the capacity of oocytes to extrude the first polar body (PB). For controls, first PB extrusion efficiency was greatly reduced for those oocytes that had undergone their GVBD late, suggesting a reduced overall fitness. In contrast, we did not observe such a difference for early versus late GVBD $Setdb1^{-/-}$ oocytes, arguing that the delay in GVBD in $Setdb1^{-/-}$ oocytes does not necessarily prevent meiotic progression (Fig. 2B).

To assess the progression of oocytes from MI to MII, we stained meiotic spindles for alpha-tubulin and DNA with DAPI. We observed that meiotic progression was affected in 30% (24/79) of $Setdb1^{-/-}$ oocytes (9/54 for early and 15/25 for late

Development (2016) 143, 2767-2779 doi:10.1242/dev.132746

A

Females	Males	Successful breeding performance (n)	Litter size +/- sd
Setdb1 $^{f/f}$	*Setdb1* $^{f/f}$	100% (7)	7.4 +/- 2.3
Setdb1 $^{f/+}$; *Zp3*-cre	*Setdb1* $^{f/f}$	100% (7)	7.7 +/- 2.9
Setdb1 $^{f/f}$; *Zp3*-cre	*Setdb1* $^{f/f}$	0% (7)	0

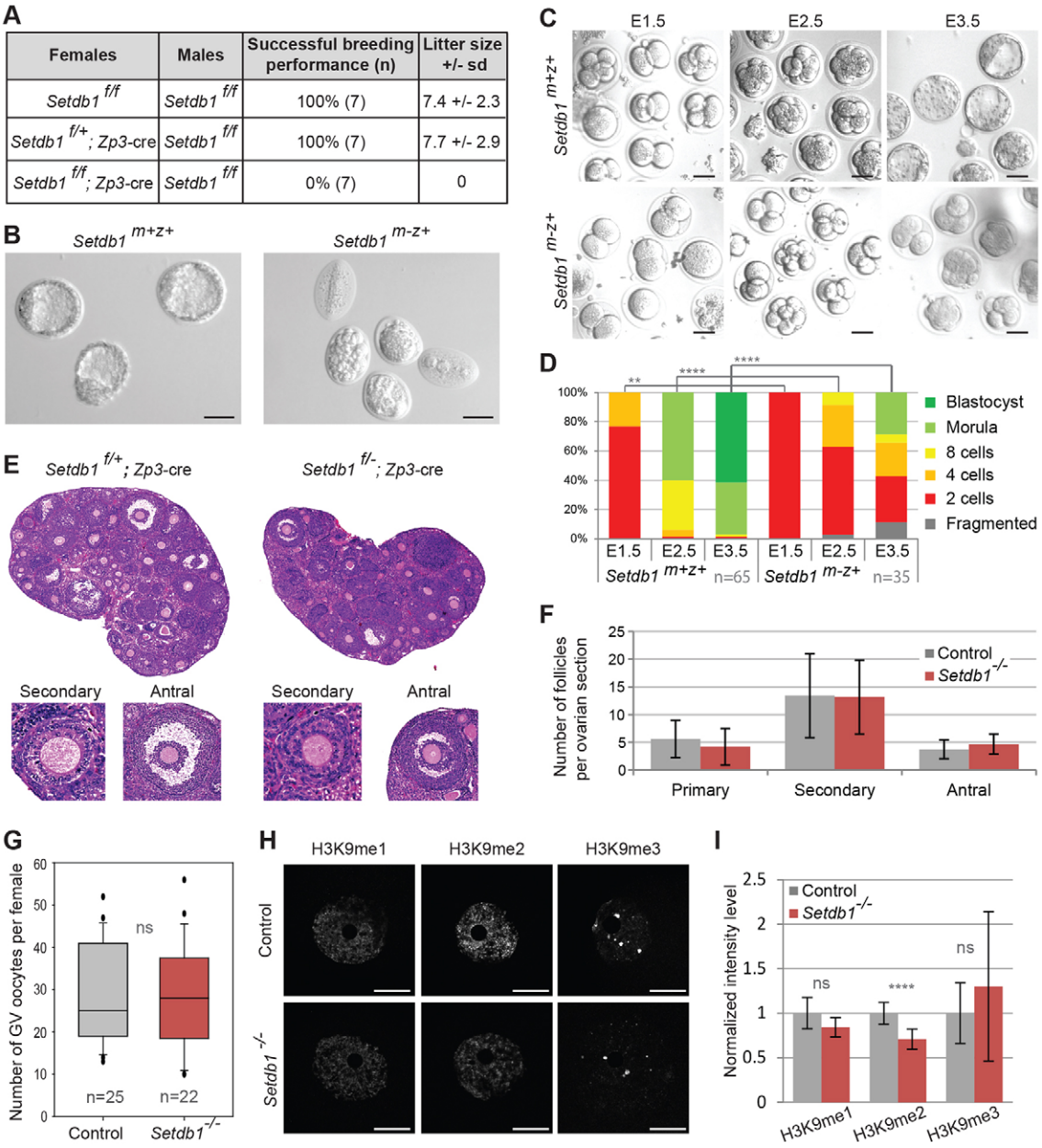

Fig. 1. Loss of maternal *Setdb1* impairs early embryonic development but not folliculogenesis. (A) 8-12-week-old control (*Setdb1*$^{f/f}$ and *Setdb1*$^{f/+}$; *Zp3*-cre) and *Setdb1* mutant (*Setdb1*$^{f/f}$; *Zp3*-cre) females were crossed with control (*Setdb1*$^{f/f}$) males. Litter sizes were determined on the first three litters. *n*, number of breeding pairs, s.d., standard deviation. (B) Differential interference contrast (DIC) images of *Setdb1*$^{m+z+}$ and *Setdb1*$^{m-z+}$ embryos flushed from uteri at E3.5. (C,D) *In vitro* embryonic development of *Setdb1*$^{m+z+}$ and *Setdb1*$^{m-z+}$ embryos (E1.5 to E3.5). (C) Representative DIC images. (D) Frequencies of developmental progression of *Setdb1*$^{m+z+}$ and *Setdb1*$^{m-z+}$ embryos that developed beyond the first cleavage. *n*, number of embryos analyzed. *P*-values were calculated with a Chi-square test. $^{**}P<0.01$; $^{****}P<0.0001$. (E) Hematoxylin and Eosin staining of ovarian sections from 2-month-old females. (F) Classification of follicles per ovarian section (six sections per ovary for three mice per genotype were analyzed). (G) Box plot showing number of GV oocytes collected per female [central bar, median; lower and upper box limits, 25th and 75th percentiles, respectively; whiskers, 5th (bottom) and 95th (top) percentile; dots indicate outliers]. *n*, number of mice analyzed. ns, non-significant by *t*-test. (H) H3K9 methylation staining on GV oocytes. (I) 3D quantification of mono-, di- and tri-H3K9 methylation levels relative to histone levels in oocytes. *n*=3, 10, 9 control and *n*=9, 11, 13 mutant oocytes for the respective methylations. Data represented as mean±s.d. *P*-values were calculated with an unpaired *t*-test assuming equal variance. $^{****}P<0.0001$; ns, non-significant. Scale bars: 50 µm in B,C; 20 µm in H.

GVBDs), compared with only 1.3% (1/79) for control oocytes (Fig. 2C). *Setdb1*$^{-/-}$ oocytes displayed various chromosome defects such as misaligned chromosomes, presence of multiple spindles, chromosome bridges in anaphase and, more surprisingly, chromosome decondensation and formation of pronuclei-like structures (Fig. 2D). Classification of all defects revealed that both metaphase stages were affected in *Setdb1*$^{-/-}$ oocytes and that the defects were more pronounced in oocytes with delayed GVBD (Fig. 2C-E). In the early GVBD class of oocytes, MI and MII oocytes were equally affected, showing misaligned chromosomes or the presence of multiple spindles. In the late GVBD class of oocytes, the majority of abnormal oocytes displayed defects in the progression from MI to MII, at anaphase I, telophase I and cytokinesis. In addition, we observed the presence of pronuclei-like structures that form after the first meiotic division; an observation confirmed by live imaging (Fig. 2F; Movies 1 and 2). In *Setdb1*$^{-/-}$

Development (2016) 143, 2767-2779 doi:10.1242/dev.132746

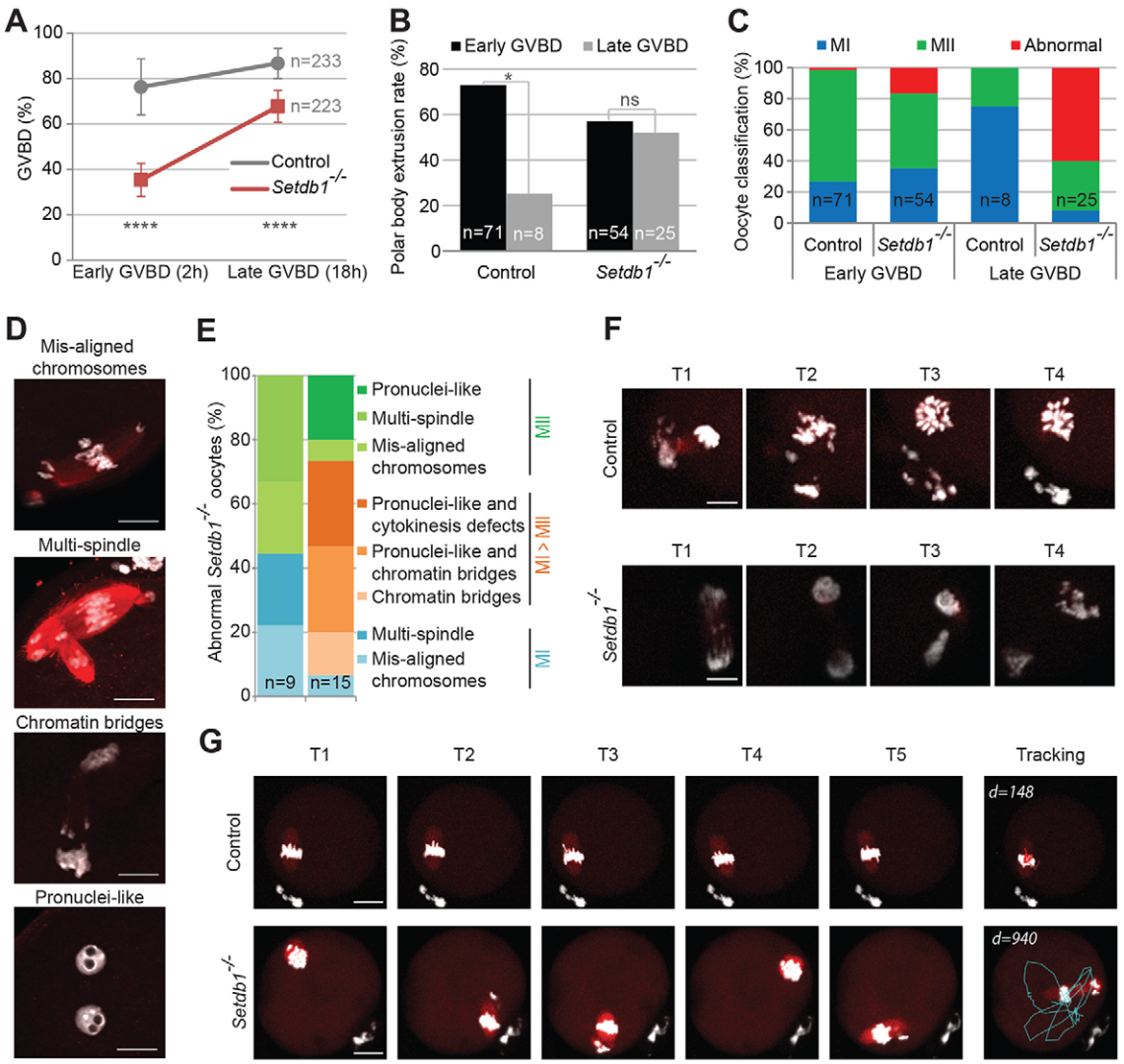

Fig. 2. Loss of *Setdb1* impairs meiotic maturation. (A) Percentage of GV breakdown (GVBD) at 2 h and 18 h after milrinone removal in control and *Setdb1*$^{-/-}$ embryos. Mean±s.d. ****P<0.0001, Chi-square test. (B) Polar body extrusion rate in control and *Setdb1*$^{-/-}$ embryos at early or late GVBD, respectively, before or 2 h after milrinone removal. *P<0.05, Chi-square test; ns, non-significant. (C) Meiotic maturation analysis of control and *Setdb1*$^{-/-}$ oocytes after early or late GVBD. Oocytes were classified as MI, MII or abnormal based on chromosome morphology and alignment as well as polar body extrusion. (D) Images of abnormal *Setdb1*$^{-/-}$ oocytes stained with anti-alpha-tubulin (red) and DAPI (gray). (E) Classification of abnormal *Setdb1*$^{-/-}$ oocytes from Fig. 2C. Blue, oocytes in MI; orange, oocytes between MI and MII; green, oocytes in MII. (F,G) Control and *Setdb1*$^{-/-}$ GV oocytes were micro-injected with transcripts encoding for H2B-mCherry (gray) and alpha-tubulin (red). Meiotic maturation was followed by live imaging (see Movies 1 and 2). (F) Selection of time points around anaphase I. (G) Selection of time points after first PB extrusion (with 60 min between each time point). Far right panels show tracking of spindles in projected *x-y* plane using Ilastik box (in red for control and blue for *Setdb1*$^{-/-}$ oocytes). *d*, distance movement of spindles (arbitrary unit); *n*, number of oocytes analyzed. Scale bars: 20 µm.

oocytes, extrusion of the first PB was followed by a phase of chromosome decondensation and recondensation, suggesting a short interphase-like period before re-entry in MII. We never observed this behavior in control oocytes.

Live imaging also revealed that misaligned chromosomes might even be a more common feature of *Setdb1*$^{-/-}$ oocytes (Fig. 2G; Movies 1 and 2). Depending on the timing of fixation, chromosomes appear perfectly aligned on the metaphase plate, or not (Fig. 2G, compare T4 and T5, for instance). Interestingly, extrusion of the first PB in a *Setdb1*$^{-/-}$ oocyte was followed by a meiotic spindle that moved erratically in the cytoplasm (Fig. 2G; Movies 1 and 2). In contrast, the spindle of the control oocyte was stably positioned at the periphery of the cell, near the extrusion site of the first PB, indicating stable anchorage to the cortex of the oocyte. The latter data suggest that Setdb1 might control asymmetrical positioning and anchoring of the meiotic spindle in oocytes. Together, these results demonstrate that *Setdb1* expression during oocyte growth is required for proper meiotic maturation and various processes driving meiotic chromosome segregation.

Loss of *Setdb1* impairs kinetochore-microtubule interactions and spindle organization

To investigate in more detail whether the observed phenotypes were associated with defects in chromosome condensation and/or cohesion and would lead to actual chromosome mis-segregation, we generated chromosome preparations of MI and MII oocytes (Fig. 3A). We did not observe any defects in chromosome structure, nor in arm and centromeric cohesion at the first and secondary

Development (2016) 143, 2767-2779 doi:10.1242/dev.132746

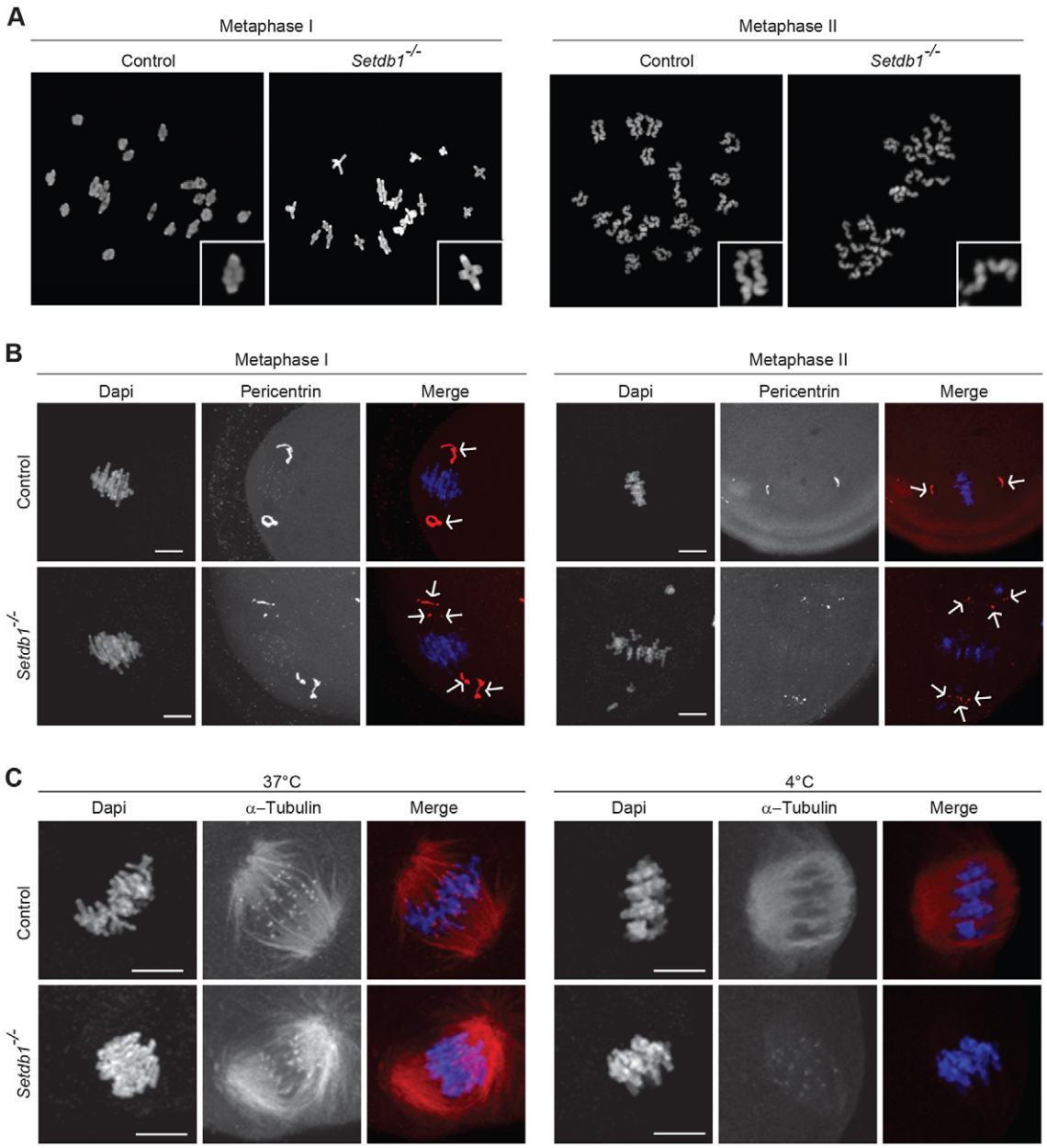

Fig. 3. Bipolar spindle organization and kinetochore-spindle interaction are disturbed upon loss of *Setdb1*. (A) Metaphase spreads of MI and MII oocytes, stained with DAPI. Boxes show magnification of bivalent (MI) or monovalent (MII) chromosomes (MI: *n*=5 control and *n*=11 *Setdb1*$^{-/-}$; MII: *n*=5 control and *n*=15 *Setdb1*$^{-/-}$ oocytes analyzed). (B) Detection of microtubule organization centers (MTOC; arrows) by immunofluorescence with anti-pericentrin antibody (red) (*n*=10 control and *n*=8 *Setdb1*$^{-/-}$ oocytes analyzed). (C) Stability of the kinetochore-spindle interaction was tested at 37°C and after a cold treatment at 4°C. Spindle was detected by immunofluorescence with an antibody against alpha-tubulin (red). Signals at kinetochores represent immunostaining with anti-Crest antibodies (*n*=17 and 5 control; and *n*=8 and 13 *Setdb1*$^{-/-}$ oocytes analyzed at 37°C and 4°C, respectively). Scale bars: 20 µm.

division of *Setdb1*$^{-/-}$ oocytes, respectively. Nonetheless, 4/13 *Setdb1*$^{-/-}$ MII oocytes were aneuploid, arguing for reasons other than defects in chromatin and cohesion dynamics underlying the chromosome segregation defects occurring in the first meiotic division.

Indeed, our previous analyses indicate that spindle organization is abnormal in *Setdb1*$^{-/-}$ oocytes (Fig. 2D). In oocytes, multiple MTOC form and cluster together to organize a bipolar spindle (Schuh and Ellenberg, 2007). To study MTOC clustering in control and *Setdb1*$^{-/-}$ oocytes, we used an antibody against pericentrin, which is a core component of MTOCs (Fig. 3B). We invariably detected pericentrin staining at two spindle poles in all control oocytes. However, 5/8 of *Setdb1*$^{-/-}$ oocytes showed a defect in MTOC clustering, which might underlie the formation of multiple spindles described above.

We also tested the attachment of microtubules to kinetochores in *Setdb1*$^{-/-}$ oocytes. In response to a short exposure to cold temperature, microtubules usually disassemble, with the exception of those spindle microtubules that are stably attached to kinetochores. We exposed control and *Setdb1*$^{-/-}$ oocytes to cold and performed staining for alpha-tubulin (Fig. 3C). Cold treatment did not affect the spindle morphology in control oocytes, consistent with the presence of stable kinetochore-microtubule attachments. In contrast, 3/13 *Setdb1*$^{-/-}$ oocytes displayed weak spindles with some chromosomes unattached. More strikingly, the spindle was undetectable in the remaining 10

Development (2016) 143, 2767-2779 doi:10.1242/dev.132746

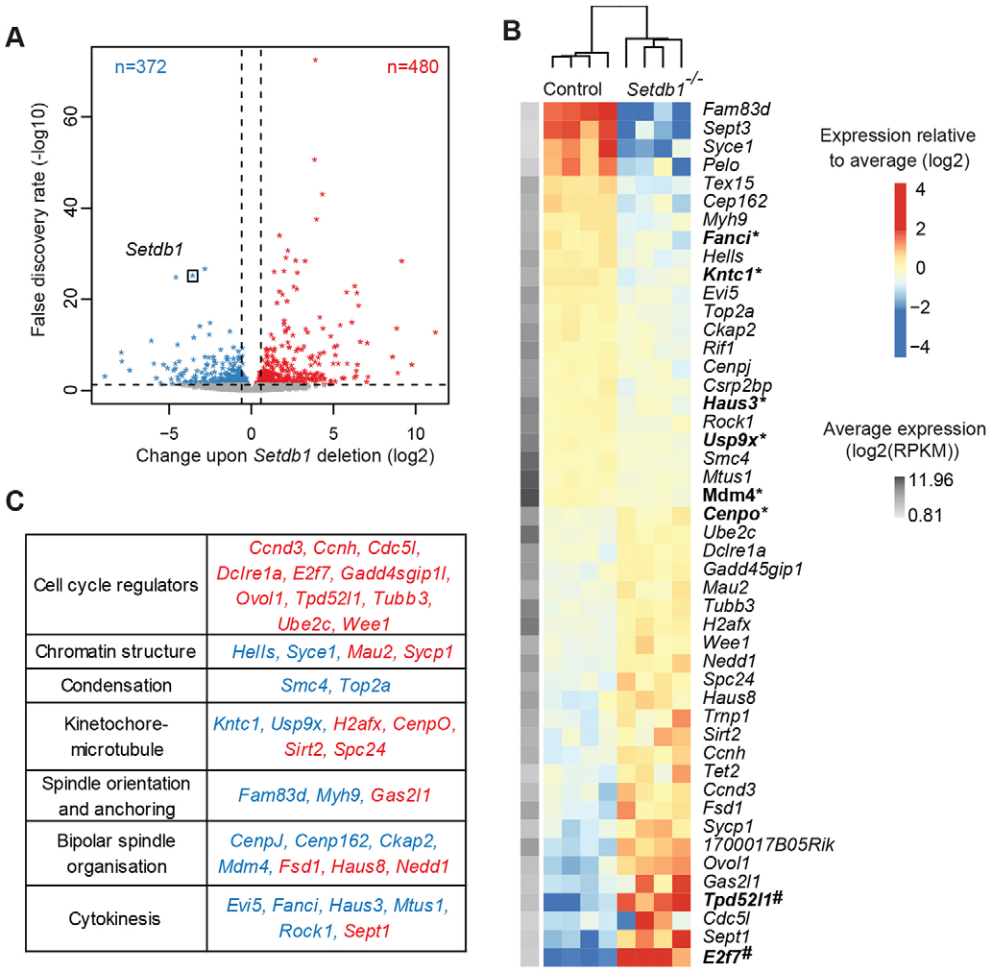

C

Cell cycle regulators	*Ccnd3, Ccnh, Cdc5l, Dclre1a, E2f7, Gadd4sgip1l, Ovol1, Tpd52l1, Tubb3, Ube2c, Wee1*
Chromatin structure	*Hells, Syce1, Mau2, Sycp1*
Condensation	*Smc4, Top2a*
Kinetochore-microtubule	*Kntc1, Usp9x, H2afx, CenpO, Sirt2, Spc24*
Spindle orientation and anchoring	*Fam83d, Myh9, Gas2l1*
Bipolar spindle organisation	*CenpJ, Cenp162, Ckap2, Mdm4, Fsd1, Haus8, Nedd1*
Cytokinesis	*Evi5, Fanci, Haus3, Mtus1, Rock1, Sept1*

Fig. 4. Gene expression changes upon *Setdb1* depletion relate to the phenotype. (A) Volcano plot showing upregulated (red) and downregulated (blue) genes in *Setdb1*-deficient GV oocytes (FDR<0.05). (B) Heatmap showing average expression for all replicates and relative expression between replicates for genes with cell cycle and division functions (based on GO-term). *, presence of splice junctions between ERVs and exons in genes, independently of *Setdb1* expression. #, presence of splice junctions between ERVs and exons in genes, with increased expression upon *Setdb1* deletion. See also Fig. 5 and Table S1. (C) Functional classification of upregulated (red) and downregulated (blue) genes associated with cell cycle- and division-related functions according to GO term analyses.

Setdb1$^{-/-}$ oocytes. This experiment suggests that spindle microtubules are not stably attached to kinetochores in absence of *Setdb1*.

Improperly attached kinetochores activate the spindle assembly checkpoint (SAC). To test whether the SAC was properly activated in *Setdb1*$^{-/-}$ oocytes, we treated GV oocytes with nocodazole, a microtubule-depolymerizing agent. If the SAC was defective in *Setdb1*$^{-/-}$ oocytes, they should be able to overcome the MI arrest induced by nocodazole. Both control and *Setdb1*$^{-/-}$ oocytes were arrested in MI upon nocodazole treatment, suggesting that SAC is activated in absence of *Setdb1* (data not shown). These results demonstrate the importance of *Setdb1* expression during oogenesis for ensuring the formation of a bipolar spindle, stable kinetochore-microtubule attachment and accurate chromosome segregation during meiosis.

Setdb1 controls gene expression during oogenesis

Given the known function of Setdb1 in gene regulation, we anticipated that its deficiency during oocyte growth would alter expression of genes controlling meiotic maturation and chromosome segregation. To test this hypothesis, we performed genome-wide expression profiling on mutant (*Setdb1*$^{f/-}$; *Zp3*-cre) oocytes and two different groups of control oocytes (*Setdb1*$^{f/-}$ and *Setdb1*$^{f/+}$; *Zp3*-cre), enabling correction for transcriptional effects by *Zp3*-cre transgene expression during oogenesis (Fig. S2A). We found 480 and 372 genes to be up- and downregulated, respectively, upon disruption of the *Setdb1* gene, with *Setdb1* being one of the most significantly downregulated genes (Fig. 4A; Fig. S2B, Table S1).

Gene ontology (GO) analyses of mis-regulated genes revealed overrepresentation of several biological processes, including functions in cell cycle and cell division (Fig. S2C). Among upregulated genes, many have been implicated in cell cycle control (Fig. 4B,C). For example, *Ube2c* encodes a ubiquitin-conjugating enzyme known to regulate mitotic exit by promoting cyclin B degradation (Ben-Eliezer et al., 2015; Hao et al., 2012). Moreover, overexpression of the kinase *Wee1* might delay cell cycle progression in oocytes and early embryos that is normally controlled by Wee1b and/or Wee2 (Han et al., 2005; Liu et al., 2013).

Other mis-regulated genes have been implicated in chromosome condensation, kinetochore-spindle attachment, heterochromatin structure, organization of a bipolar spindle, regulation of spindle orientation and cytokinesis (Fig. 4B,C). Their mis-regulation might contribute to the phenotypes observed in *Setdb1*$^{-/-}$ oocytes. For instance, *Kntc1* (kinetochore associated 1) is a component of the evolutionarily conserved Rod-Zwilch-Zw10 (RZZ) complex required for a stable kinetochore-spindle attachment, mutations of which are associated with chromosome segregation defects (Karess, 2005). *Ckap2* (cytoskeleton associated protein 2) is required for the maintenance of microtubule nucleation sites and its depletion leads to multipolar mitosis, which could explain the presence of the multi-spindle and MTOC-clustering defects observed in *Setdb1*$^{-/-}$ oocytes (Case et al., 2013). Importantly, as Setdb1 is known as a transcriptional repressor, the downregulation of genes suggests that Setdb1 might control meiotic maturation by orchestrating a network of gene interactions during oogenesis.

Development (2016) 143, 2767-2779 doi:10.1242/dev.132746

Setdb1 downregulates ERVK and ERVL-MaLR expression during oogenesis

Setdb1 controls transcriptional repression of ERVK and ERV1 retrotransposons in ESCs and PGCs (Karimi et al., 2011; Liu et al., 2014). To assess a possible role of altered expression of repetitive elements in meiotic maturation and division, we analyzed their expression in *Setdb1*$^{-/-}$ and control GV oocytes according to RefSeq annotation. *Setdb1* deficiency during oocyte growth caused a 1.5-fold upregulation of repeats, with 18% of all reads mapping to repetitive elements in *Setdb1*$^{-/-}$ oocytes, compared with 12% in controls (data not shown). Primarily LTR retrotransposons belonging to ERVL-MaLR and ERVK families were upregulated, in addition to some ERV1, ERVL, SINE B2 and GSAT_MM satellite sequences (FDR<0.05) (Fig. 5A,B; Tables S2 and S3).

In wild-type oocytes, ERVL-MaLRs contribute most highly to overall retrotransposon expression (Fig. 5B), as reported previously (Fadloun et al., 2013). Intriguingly, *Setdb1* deficiency enables further upregulation of the already highly expressed MTA, MTB and MLT elements, as well as of more moderately expressed ORR1 elements. Likewise, expression of 46 families of ERVKs was upregulated upon *Setdb1* depletion, including ETn, ERVB7 (MusD), IAPd, IAPEz, MMERVK10C and RLTR45, which are silenced in a *Setdb1*-dependent manner in ESC (Fig. 5C; Table S3) (Karimi et al., 2011). Thus, in contrast to ESCs, these data identify Setdb1 as a negative modulator of ERVK and ERVL-MaLR expression rather than a strong repressor of ERV transcription during oogenesis.

We next wondered whether induction of ERV transcription by *Setdb1* depletion could promote transcription of nearby genes. Towards this, we identified and quantified sequence reads that consisted of the 5′ end of ERV and 3′ end of gene exon sequences, hereafter referred to as splice junctions. We classified such splice junctions into three groups, 'upstream', 'within' and 'downstream', according to the location of the ERV relative to the exon of an associated open reading frame (ORF). We also quantified splice junctions between ERVs and non-exonic sequences. We determined the levels of altered expression at such splice junctions upon *Setdb1* deletion (Fig. 5D; Table S4). For ERVL-MaLR, over 48% of splice junctions involving an ERV occurred in the context of an annotated ORF, whereas for ERVK this was 24% (Fig. 5D). These data support a role of ERVL-MaLR and ERVK in driving gene expression in oocytes.

For both ERV classes, over 5% of splice junctions with the ERV localized upstream of the annotated exon were upregulated in *Setdb1*$^{-/-}$ oocytes, indicating that Setdb1 suppresses ERV-driven gene transcription (Fig. 5D,E). In addition, ∼11% of splice junctions originating from ERVs within an ORF were upregulated in *Setdb1* mutant oocytes, likely representing aberrant non-functional chimeric transcripts (Fig. 5D). Among the upregulated genes involved in cell cycle regulation and cell division, we measured for *E2f7* (Fig. S3A) and *Tpd52l1* increased expression of splice junctions, but only for those initiated from 3′ localized ERVs, linked to downstream exons.

To further enhance the likelihood of identifying ERV-induced gene expression impairing meiosis and mitosis, we related our RNA sequencing data to a recent annotation of the mouse oocyte transcriptome characterized by prominent ERV-driven gene expression (Veselovska et al., 2015). Indeed, we measured an increase of over tenfold in expression of ERV-induced transcripts in control and *Setdb1* mutant oocytes, compared with RefSeq annotation (Fig. S3B). These analyses confirmed expression of ERV-initiated chimeric transcripts for *E2f7* and *Tpd52l1* and identified chimeric transcripts for *1700017B05Rik* with unknown functions (Table S5). Finally, we did not observe increased levels of phosphorylated H2A.X, a marker of DNA damage, in *Setdb1* mutant oocytes (Fig. S4A,B).

In summary, we conclude that Setdb1 restricts but does not prevent ERVK- and ERVL-MaLR-driven gene expression. We anticipate that the contribution of such expression to the meiotic maturation and division phenotype is limited as most relevant splice junction events initiated from ERVs are within genes, thereby limiting the potential for the generation of functional proteins.

PKA signaling is impaired upon *Setdb1* depletion

Besides its role in meiotic maturation, *Setdb1* regulated GVBD and thus the exit from meiotic arrest (Fig. 2A). Interestingly, using Ingenuity Pathway Analysis, we identified PKA signaling as a mis-regulated pathway upon *Setdb1* deletion. Twenty-two genes belonging to the PKA signaling pathway were mis-regulated in *Setdb1*$^{-/-}$ oocytes, including *Prkaca*, which encodes one catalytic subunit of PKA (Fig. 6A). It is well-established that PKA maintains meiotic arrest in response to high levels of cAMP (Fig. 6B). To test whether the PKA pathway is actually involved in the GVBD delay observed in *Setdb1*$^{-/-}$ oocytes, we inhibited PKA using the cAMP antagonist 8-bromo-Rp-cAMP (Rp-cAMP). We first observed that Rp-cAMP overcame the milrinone-induced GV arrest in control and *Setdb1*$^{-/-}$ oocytes, demonstrating activity of the compound (Fig. S5). After removal of milrinone, Rp-cAMP treatment did not further increase the high efficiency of GVBD in control oocytes (Fig. 6C). In *Setdb1*$^{-/-}$ oocytes, however, we observed a complete alleviation of the delay in GVBD (Fig. 6C). These results suggest that GVBD delay observed in absence of *Setdb1* is due to an impairment of the PKA signaling pathway.

Cell cycle progression and chromosome segregation are impaired in *Setdb1*$^{m-z+}$ embryos

We then wondered whether the maternal deficiency of *Setdb1* would cause similar defects in early embryos as observed in meiosis. We analyzed the first embryonic cleavage by isolating *Setdb1*$^{m+z+}$ and *Setdb1*$^{m-z+}$ zygotes at E0.5 and culturing them *in vitro* for 24 h. Whereas all control zygotes developed into 2-cell embryos, only 25% (3/12) of *Setdb1*$^{m-z+}$ zygotes reached the 2-cell stage (Fig. 7A,B). Moreover, these 2-cell embryos were abnormal and contained micronuclei, suggesting defects in chromosome segregation. Interestingly, several *Setdb1*$^{m-z+}$ arrested zygotes contained pronuclei with aberrant morphologies, indicative of a failure in NEBD. By live imaging of *Setdb1*$^{m-z+}$ zygotes we saw that although the two parental pronuclei move into close proximity of each other, their nuclear envelopes never break down and the embryos arrest at the G2/M transition (Fig. 7C; Movies 3 and 4). In summary, we observed comparable defects in the G2/M transition and subsequent progression through meiosis and during the first cleavage division in response to *Setdb1* maternal deficiency. It is likely that similar defects contribute to the arrest of *Setdb1*$^{m-z+}$ embryos observed at subsequent embryonic stages (Fig. 1).

DISCUSSION

Meiotic and embryonic developmental competencies rely on a proper maturation of the oocyte, which includes synthesis and accumulation of necessary transcripts and proteins. This study reveals that the lysine methyltransferase *Setdb1* participates in the establishment of meiotic and embryonic developmental competencies. Transcriptional profiling shows that during oogenesis *Setdb1* regulates the expression of a substantial number

Development (2016) 143, 2767-2779 doi:10.1242/dev.132746

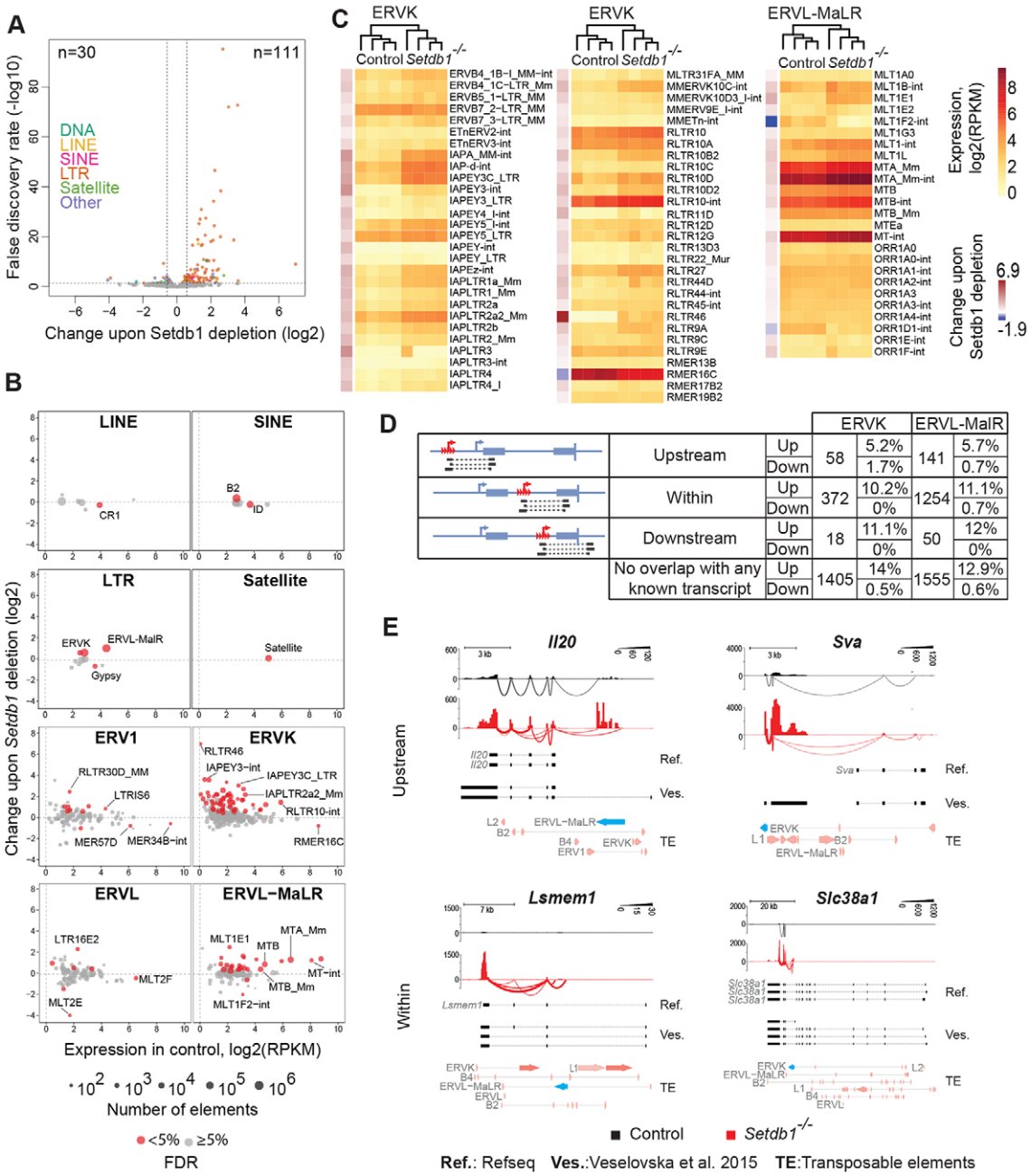

Fig. 5. *Setdb1* controls expression of repeats. (A) Volcano plot showing false discovery rates and relative expression changes of differentially expressed repClass groups upon *Setdb1* depletion in GV oocytes (FDR<0.05). (B) MA plots showing relative expression changes of different repName groups upon *Setdb1* deletion relative to their absolute expression in control oocytes. (C) Heat maps showing absolute expression of ERVs (including multi-mapped reads) for all replicates [log2(RPKM)] and fold-change (log2) between genotypes for ERVK and ERVL-MaLR repNames (FDR<0.05). (D) Number of splice junctions measured between individual ERVK or ERVL-MaLR elements and exons or other genomic locations, categorized according to location of the ERV relative to the ORF of the gene ('Upstream', 'Within', 'Downstream'). Percentages of splice junctions differentially expressed between *Setdb1*$^{-/-}$ and control oocytes are indicated. (E) Genome browser views illustrating expression along *Il20*, *Lsmem1*, *Sva* and *Slc38a1* loci (uniquely mapped reads per 100 base pair bins, library-size normalized) and expression at splice junctions (uniquely mapped reads per splice junction, library-size normalized) between ERVL-MaLR or ERVK elements and exons in control and *Setdb1*$^{-/-}$ oocytes. Splicing events occurred either with ERVs positioned upstream of or within the ORF (colored in blue), resulting in formation of chimaeric transcripts encoding for intact or likely aberrant proteins, respectively.

of genes with putative functions in meiotic maturation and early embryogenesis.

We show that the transition from prophase to metaphase, marked by GVBD, is delayed in *Setdb1*$^{-/-}$ oocytes. Meiotic arrest in prophase is normally maintained by high levels of cAMP that stimulate PKA activity, which in turn suppresses the MPF activity. Meiotic resumption is triggered by cAMP hydrolysis resulting from increased PDE3A activity in response to LH-mediated reduction in paracrine cGMP signaling from the granulosa cells (Norris et al., 2009; Vaccari et al., 2009) (Fig. 6B). In *Setdb1*$^{-/-}$ oocytes, *Prkaca* is upregulated and we demonstrate that inhibition of PKA by the cAMP antagonist Rp-cAMP fully rescues the GVBD delay, showing that *Setdb1* controls GVBD by regulating the PKA pathway. Ingenuity Pathway Analysis of expression profiling data

Development (2016) 143, 2767-2779 doi:10.1242/dev.132746

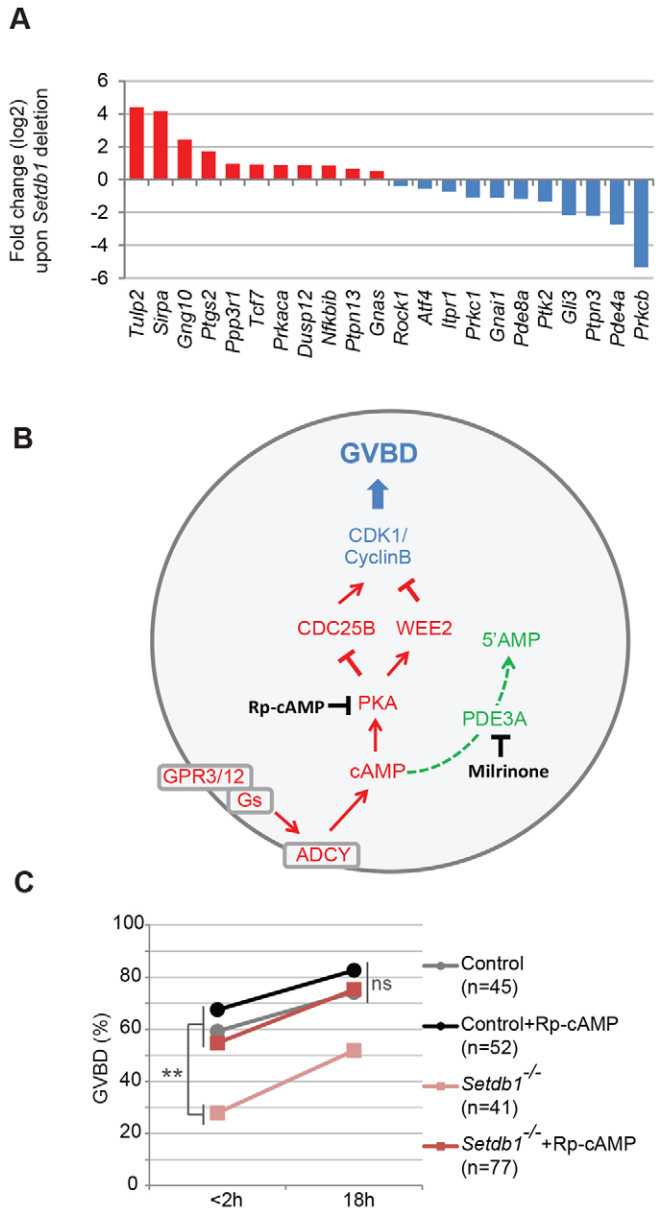

Fig. 6. PKA signaling is impaired upon *Setdb1* depletion. (A) Mis-regulation of genes associated with PKA pathway signaling in *Setdb1* mutant oocytes. Blue, downregulated genes; red, upregulated genes. (B) Scheme of pathways controlling GVBD. Green, PDE3A pathway; red, PKA pathway. Milrinone and Rp-cAMP are inhibitors of PDE3A and PKA, respectively (modified from Su et al., 2012). (C) Percentage of GVBD at 2 h and 18 h after milrinone removal for oocytes treated with or without Rp-cAMP. *n*: number of oocytes analyzed. *P*-values were calculated with a Chi-square test, $^{**}P<0.01$; ns, non-significant.

furthermore reveals that several other components of the PKA pathway are mis-expressed. For example, *Prkcb* (protein kinase C beta) is strongly downregulated in *Setdb1*$^{-/-}$ oocytes. During mitosis, Prkcb mediates phosphorylation-dependent lamin B1 disassembly, and inhibition or depletion of Prkcb delays nuclear envelope breakdown (Mall et al., 2012). Possibly, reduced *Prkcb* expression might contribute to the delayed GVBD observed in *Setdb1*$^{-/-}$ oocytes.

We frequently saw transient formation of pronuclei-like structures during the MI-to-MII transition of those *Setdb1*$^{-/-}$ oocytes that displayed a delayed onset of GVBD. Interestingly, whereas completion of meiosis I requires a reduction in MPF activity, its re-establishment is necessary to maintain chromosome condensation in MII oocytes (Brunet and Maro, 2005). Inactivation of MPF in MII oocytes was shown to induce formation of pronuclei-like structures (Madgwick et al., 2006). Thus, the appearance of a short interphase between MI and MII might result from a sustained reduction of MPF activity upon completion of meiosis. Besides PKA signaling, MPF activity is controlled by ubiquitin-mediated degradation of cyclin B by the anaphase promoting complex/cyclosome (APC/C). *Ube2c*, encoding the ubiquitin-conjugating enzyme and partner of APC/C known to promote cyclin B degradation, is upregulated in *Setdb1*$^{-/-}$ oocytes (Fig. 4B) (Xie et al., 2014). MPF activity might thus be impaired in *Setdb1*$^{-/-}$ oocytes partly as a result of an increased degradation of cyclin B by Ube2c.

We observe that in the absence of *Setdb1*, the formation of meiotic spindle is compromised by defective MTOC clustering. Moreover, unstable kinetochore-microtubule attachments likely drive the chromosome segregation defects observed in *Setdb1*$^{-/-}$ MII oocytes. In some mutant oocytes, the meiotic spindle moves dramatically throughout the cell, which likely results from a defect in anchorage of the spindle to the cortex, a process that normally ensures a proper asymmetric division (Azoury et al., 2008; Chaigne et al., 2012; Schuh and Ellenberg, 2008). We have shown that these later phenotypes correlate with changes in gene expression e.g. of *Kntc1* and *Ckap2*. Intriguingly, several of the cell cycle and division genes are downregulated in the absence of *Setdb1*. Since Setdb1 is known to function as a transcriptional repressor, a secondary mechanism might be involved in which depletion of *Setdb1* would induce the upregulation of transcriptional repressors.

Setdb1$^{-/-}$ MII oocytes can be successfully fertilized; nevertheless, maternally deficient embryos arrest early during pre-implantation development, substantially prior to the lethality of *Setdb1* zygotically null embryos occurring after implantation (Dodge et al., 2004). Thus, maternal *Setdb1* is crucial for embryonic development. Indeed, similar to mutant oocytes, NEBD at the G2/M transition and chromosome segregation are severely impaired in *Setdb1*$^{m-z+}$ embryos. The presence of one large pronucleus in arrested *Setdb1*$^{m-z+}$ zygotes indicates that NEBD does ultimately occur, yet is followed by syngamy without chromosome segregation. Some *Setdb1*$^{m-z+}$ embryos went through the first cleavage division, but these embryos displayed chromosome segregation defects. Given that the meiosis-to-mitosis transition is mechanistically a gradual process lasting over many cleavage divisions (Courtois et al., 2012; Cui et al., 2008; Poueymirou and Schultz, 1987; Yu et al., 2008), we propose that the observed defects in G2/M transition and mitosis underlie the arrest of *Setdb1*$^{m-z+}$ embryos at successive stages of pre-implantation development.

Besides the transcriptional regulatory function during oogenesis, we cannot exclude a post-transcriptional role of Setdb1 in meiosis by modifying proteins directly (Fei et al., 2015; Kaustov et al., 2011; Van Duyne et al., 2008). Identifying such Setdb1 targets in oocytes, however, is a challenging prospect.

Finally, we identify *Setdb1* as a modulator of ERVL-MaLR and ERVK expression during oogenesis. *Setdb1*-mediated H3K9me3 and DNA methylation have been implicated in the silencing of LTR elements in undifferentiated and differentiated cells, respectively (Hutnick et al., 2010; Matsui et al., 2010; Walsh et al., 1998). *Setdb1* controls H3K9me3 deposition at and silencing of several class I ERV1 and class II ERVK retrotransposons in ESCs, PGCs and in

Development (2016) 143, 2767-2779 doi:10.1242/dev.132746

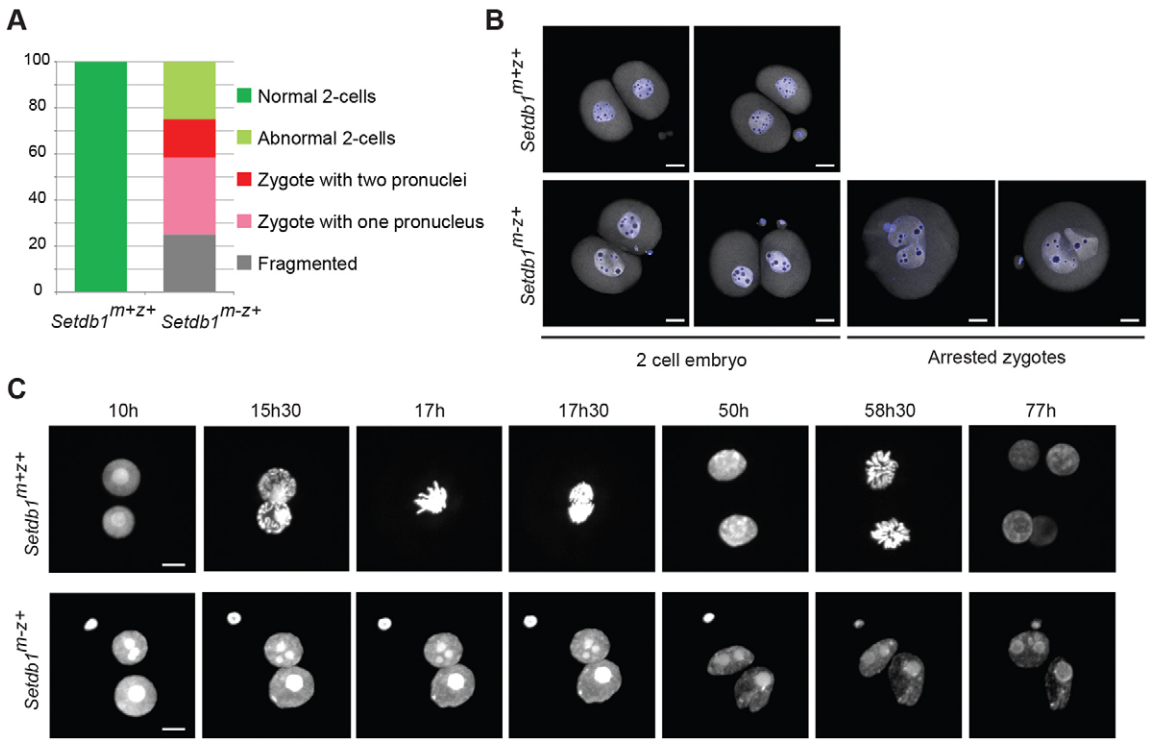

Fig. 7. Cell cycle progression and chromosome segregation are impaired in *Setdb1*$^{m-z+}$ embryos. (A) *In vitro* development of *Setdb1*$^{m+z+}$ (*n*=4) and *Setdb1*$^{m-z+}$ (*n*=12) embryos during the first cleavage. (B) Representative images of control and *Setdb1*$^{m-z+}$ 2-cell embryos (with micronuclei) and of arrested *Setdb1*$^{m-z+}$ zygotes. Embryos were stained with DAPI (blue) and CREST (gray). (C) Time lapse of first two mitotic divisions. MII oocytes were micro-injected with H2B-mCherry (gray) followed by intra-cytoplasmic sperm injection (ICSI). First cleavage was then followed by live imaging (see Movies 3 and 4). Time after ISCI is indicated. Scale bars: 20 µm.

fetal brain (Karimi et al., 2011; Liu et al., 2014; Tan et al., 2012). In contrast, ERVL-MaLR elements lack H3K9me3 occupancy in wild-type ESCs and PGCs, and fail to be upregulated upon *Setdb1* deletion (Karimi et al., 2011; Liu et al., 2014; Matsui et al., 2010; Tan et al., 2012). During oogenesis, however, many ERVK elements that are typically silenced by *Setdb1* in ESCs and PGCs are already expressed. Analysis of splice junctions involving individual elements shows that loss of *Setdb1* further enhances the expression of already active elements while also enabling derepression of other ERVK elements. The mechanistic details underlying such cell type- and ERVK element- specific modulatory roles of *Setdb1* in catalyzing H3K9me2 and/or H3K9me3 and in controlling repression are, however, not understood. We cannot exclude possible heterogeneity in H3K9 methylation levels at different elements leading potentially to 'variegated' expression levels of individual elements in different oocytes. In addition or alternatively, possible variegated or lack of ERV repression might relate to the rather low to moderate expression of the two KRAB-containing zinc finger proteins Zfp932 and Gm15446 in wild-type GV oocytes. These KRAB-ZFPs have recently been shown to control repression of various ERVK elements, known to also be silenced by Kap1 (also known as Trim28 or Tif1beta) and Setdb1 (Ecco et al., 2016).

We also identified *Setdb1* as a negative regulator of ERVL-MaLR expression; decreasing, yet not silencing, the expression of such elements in oocytes. It remains to be determined whether its catalytic activity is required for such suppression. ERVL-MaLR and ERVK elements have been suggested to drive gene expression in oocytes and early mouse embryos (Peaston et al., 2004; Veselovska et al., 2015). For 55 out of 80 chimeric transcripts identified by Peaston and colleagues (2004) to be expressed in oocytes, we confirmed the presence of splice junctions in our expression data set, a few of which were upregulated upon *Setdb1* deficiency (Table S1). Our findings thus characterize *Setdb1* as a potential modulator of ERV-induced gene expression at the oocyte-to-embryo transition. Nonetheless, we did not obtain compelling evidence for a role of impaired ERV repression in driving gene expression associated with aberrant meiotic phenotypes. In early embryos, knockdown of *Setdb1* increased expression of retrotransposons LINE1, SINE-B2 and IAP (Hatanaka et al., 2015). Nevertheless, a role for *Setdb1* in controlling repeat-driven gene expression and development of early embryos remains to be shown.

In summary, our study reveals an essential function for the lysine methyltransferase Setdb1 in cell division. The data is in line with a transcriptional regulatory function for *Setdb1* during oocyte growth that subsequently impacts on meiosis and mitosis in mouse oocytes and early embryos. Interestingly, *Setdb1* deficiency in mouse neuronal progenitors was also associated with mis-regulation of genes involved in M-phase, suggesting that Setdb1 regulates expression of genes involved both in meiosis and mitosis, and even in somatic cells (Tan et al., 2012).

MATERIALS AND METHODS

Mice

Mice maternally deficient for *Setdb1* were generated by crossing *Setdb1*$^{f/f}$ mice (Lohmann et al., 2010) with *Zp3*-cre transgenic mice to induce deletion in growing oocytes. Mice were maintained on a C57Bl/6J genetic background. All experiments were performed according to Swiss animal protection laws and institutional guidelines.

Development (2016) 143, 2767-2779 doi:10.1242/dev.132746

Embryogenesis

Zygotes and blastocysts were harvested from superovulated females mated to control males at 18 h and 90 h after hCG injection, respectively. We cultured embryos *in vitro* using standard conditions as detailed in the supplementary Materials and Methods. We performed piezo-driven intra-cytoplasmic sperm injection as described previously (Yoshida and Perry, 2007).

Oocyte isolation and culture

GV oocytes were isolated in M2 medium containing 2.5 mM milrinone (Sigma). After milrinone washout, oocytes were cultivated in M16 (Sigma) at 37°C in controlled atmosphere. When necessary, 5 mM Rp-cAMP (Sigma B2432) and 0.04 µg/ml nocodazole (Sigma M1404) were used. For the cold treatment experiment, the zona pellucida was removed with acidic tyrode and MII oocytes cultivated for 2 h before being incubated on ice for 20 min and fixed.

Immunofluorescence staining, preparation of chromosome spreads and histology were performed as described previously (Peters et al., 2001), with modifications as described below.

Immunofluorescence

Oocytes and embryos were fixed in 4% paraformaldehyde, washed in PBT (PBS, 0.1% Tween 20), permeabilized (PBS, 0.5% Triton X-100), washed in washing solution (PBS, 2% BSA, 0.1% Tween 20), blocked (blocking solution: PBS, 2% BSA, 0.1% Tween 20, 5% goat serum) and incubated with primary antibody overnight at 4°C. After further washing in washing solution, oocytes and embryos were incubated for 1 h with secondary antibody, washed again in PBT and counterstained in Vectashield with DAPI. Antibodies used: rabbit anti-H3K9me1, H3K9me2, H3K9me3 (1:500; Peters et al., 2003), rabbit anti-H3 (1:800; Abcam, ab1791), mouse anti-nucleosome (1:1000; van der Heijden et al., 2007), mouse anti-γ-H2AX (1:1000; Millipore, 05636), mouse anti-alpha-tubulin (1:400; Sigma, T9026), human anti-crest (1:1000; Fitzgerald, 90C-C51058), mouse anti-pericentrin (1:200; BD Transduction Laboratories, 611814), mouse anti-RNA polymerase II (1:30; Covance, MMS 126R). Secondary antibodies (ThermoFisher; 1:500 unless stated otherwise): goat anti-rabbit Alexa Fluor 488 (A11034), goat anti-mouse Alexa Fluor 568 (A11031), donkey anti-rabbit Alexa Fluor 568 (A10042), donkey anti-mouse Alexa Fluor 488 (A21202), goat anti-human Alexa Fluor 633 (1:150; A21091). Acquisition of images was done with a Zeiss LSM700 confocal microscope. Intensity quantification and chromosome tracking were done using Ilastik (Interactive Learning and Segmentation Toolkit; Sommer et al., 2011) and MetaMorph (Molecular Devices) software. Intensities of H3K9me and γ-H2AX stainings were normalized to intensity of nucleosome staining.

Chromosome spreads

Chromosome spreads were generated from MI and MII oocytes respectively isolated 8 h after milrinone removal and 18 h after hCG injection. Oocytes were incubated for 6 min in hypo-buffer (0.5% Na citrate, 15% FCS), 3 s in ice-cold 5-1-3 fixative (5 parts methanol, 1 part acid acetic, 3 parts dH_2O) and transferred onto a slide. A couple of drops of ice-cold 4-4-2 fixative (4 parts methanol, 4 parts acid acetic, 2 parts dH_2O) followed by a drop of 3-1 fixative (3 parts methanol, 1 part acid acetic) were carefully added to the oocyte. The slides were dried overnight and chromosomes stained with DAPI.

Ovaries histology

Ovaries were fixed in 4% paraformaldehyde overnight at 4°C and embedded in paraffin. Sectioning was done with an automatic microtome (Microm HM355S) and Hematoxylin and Eosin staining was performed according to standard procedures.

Micro-injection and live-imaging

H2B-mCherry and tubulin-EGFP mRNA were transcribed *in vitro* (mMessage mMachine SP6/T7, Ambion) and purified (RNeasy Mini Kit, Qiagen). Cytoplasmic microinjection of 3-5 pl of mRNA (20 ng/µl H2B-mCherry and 100 ng/µl tubulin-EGFP mRNA) was performed on oocytes under a microscope (IX71, Olympus) equipped with a micromanipulator and a Femtojet (Eppendorf). For live imaging oocytes and embryos were placed in a micro-slide dish (Ibidi) with 50 µl of M16 covered by mineral oil. Time-lapse images were acquired with a spinning-disc confocal microscope (Olympus, 20× objective), at 37°C with 5% CO_2. Oocytes and embryos were imaged by multipoint acquisition function every 15 min. *z*-stacks were acquired with an interval of 3 µm.

RNA sequencing, differential gene expression and splice junction analyses

We performed expression profiling on pools of 16 denuded GV oocytes isolated per mouse. We used oocytes from four *Setdb1*$^{f/+}$; *Zp3*-cre mice and two *Setdb1*$^{f/-}$ mice as controls and oocytes from four *Setdb1*$^{f/-}$; *Zp3*-cre mice as mutant. RNA isolation and sequencing (50 cycles; single-end reads) were performed to standard procedures (see supplementary Materials and Methods). As a basis for all analyses we used the *M. musculus* genome assembly (GRCm38/mm10 December 2011), RepeatMasker repeat annotation (downloaded on 7 March 2012), RefSeq gene models (downloaded from UCSC on 4 February 2016), and the oocyte transcriptome annotation (downloaded on 29 February 2016 from the web page of the paper Veselovska et al., 2015). We performed differential gene expression and splice junction analyses according to standard operations further detailed in the supplementary Materials and Methods. Raw (fastq) and processed (bigWig) RNA sequencing data are available at GEO (GSE82002).

Note added in proof

While this manuscript was under review, Kim and colleagues (Kim et al., 2016) reported largely comparable findings on the role of maternal *Setdb1* for meiosis and embryogenesis. In addition, they observed increased mRNA and protein expression for the *Cdc14b* phosphatase, a known negative regulator of meiotic maturation (Schindler and Schultz, 2009). Using a siRNA-mediated knockdown approach, Kim et al. (2016) characterized upregulated *Cdc14b* expression as the major driver of impaired meiotic progression in *Setdb1* mutant oocytes. In our study, however, *Cdc14b* was not differentially expressed between *Setdb1*-deficient and control GV oocytes as determined by RNA sequencing analyses. This finding is surprising as both laboratories studied the same conditional deletion allele of *Setdb1* (Lohmann et al., 2010), yet on slightly different genetic backgrounds (C57Bl/6-129Sv hybrid versus C57Bl/6J). Moreover, in contrast to Kim et al. (2016), we did not perform hormonal superovulation in any of the experiments dealing with oocyte maturation. Future experiments will be required to resolve this discrepancy.

Acknowledgements

We thank T. Chen (currently at the University of Texas M.D. Anderson Cancer Center, Smithville, USA) and B. Knowles (the Jackson Laboratory, Bar Harbor, USA) for providing the *Setdb1*$^{F/F}$ and *Zp3*-cre mice, respectively. We thank T. Roloff and S. Thiry for preparation and sequencing of RNA libraries, R. Thierry for image processing and the animal facility. We thank M. Gill and M. Tardat for critical reading of the manuscript.

Competing interests

The authors declare no competing or financial interests.

Author contributions

A.E. and A.H.F.M.P. conceived and designed the experiments. A.E. performed most experiments and analyzed the data. Z.L. performed live-imaging experiments and contributed to IF experiments. Computational analyses were done by E.A.O. and M.B.S. with assistance by A.E. A.E. and A.H.F.M.P. wrote the manuscript with input of other authors.

Funding

A.E. was supported by the European Molecular Biology Organization (EMBO) Long-Term Fellowship program and by la Fondation pour la Recherche Médicale. M.B.S. was supported by the MetastasiX project of the Swiss Initiative for Systems

Biology (SystemsX.ch). Research in the A.H.F.M.P. lab was supported by the Novartis Research Foundation, the Schweizerischer Nationalfonds zur Förderung der Wissenschaftlichen Forschung (Swiss National Science Foundation) [grant numbers 31003A_125386 and NRP 63-Stem Cells and Regenerative Medicine], SystemsX.ch (Cell plasticity), the European Network of Excellence 'The Epigenome' and the EMBO YIP program.

Data availability

Raw (fastq) and processed (bigWig) RNA sequencing data are available at GEO (http://www.ncbi.nlm.nih.gov/geo/) under accession number GSE82002.

Supplementary information

Supplementary information available online at
http://dev.biologists.org/lookup/doi/10.1242/dev.132746.supplemental

References

Azoury, J., Lee, K. W., Georget, V., Rassinier, P., Leader, B. and Verlhac, M.-H. (2008). Spindle positioning in mouse oocytes relies on a dynamic meshwork of actin filaments. *Curr. Biol.* **18**, 1514-1519.

Beall, S., Brenner, C. and Segars, J. (2010). Oocyte maturation failure: a syndrome of bad eggs. *Fertil. Steril.* **94**, 2507-2513.

Ben-Eliezer, I., Pomerantz, Y., Galiani, D., Nevo, N. and Dekel, N. (2015). Appropriate expression of Ube2C and Ube2S controls the progression of the first meiotic division. *FASEB J.* **29**, 4670-4681.

Bouniol-Baly, C., Hamraoui, L., Guibert, J., Beaujean, N., Szöllösi, M. S. and Debey, P. (1999). Differential transcriptional activity associated with chromatin configuration in fully grown mouse germinal vesicle oocytes. *Biol. Reprod.* **60**, 580-587.

Brunet, S. and Maro, B. (2005). Cytoskeleton and cell cycle control during meiotic maturation of the mouse oocyte: integrating time and space. *Reproduction* **130**, 801-811.

Case, C. M., Sackett, D. L., Wangsa, D., Karpova, T., McNally, J. G., Ried, T. and Camps, J. (2013). CKAP2 ensures chromosomal stability by maintaining the integrity of microtubule nucleation sites. *PLoS ONE* **8**, e64575.

Chaigne, A., Verlhac, M.-H. and Terret, M.-E. (2012). Spindle positioning in mammalian oocytes. *Exp. Cell Res.* **318**, 1442-1447.

Cho, S., Park, J. S. and Kang, Y.-K. (2011). Dual functions of histone-lysine N-methyltransferase Setdb1 protein at promyelocytic leukemia-nuclear body (PML-NB): maintaining PML-NB structure and regulating the expression of its associated genes. *J. Biol. Chem.* **286**, 41115-41124.

Courtois, A., Schuh, M., Ellenberg, J. and Hiiragi, T. (2012). The transition from meiotic to mitotic spindle assembly is gradual during early mammalian development. *J. Cell Biol.* **198**, 357-370.

Cui, C., Zhao, H., Zhang, Z., Zong, Z., Feng, C., Zhang, Y., Deng, X., Xu, X. and Yu, B. (2008). CDC25B acts as a potential target of PRKACA in fertilized mouse eggs. *Biol. Reprod.* **79**, 991-998.

De La Fuente, R. (2006). Chromatin modifications in the germinal vesicle (GV) of mammalian oocytes. *Dev. Biol.* **292**, 1-12.

Dekel, N. (1996). Protein phosphorylation/dephosphorylation in the meiotic cell cycle of mammalian oocytes. *Rev. Reprod.* **1**, 82-88.

Dodge, J. E., Kang, Y.-K., Beppu, H., Lei, H. and Li, E. (2004). Histone H3-K9 methyltransferase ESET is essential for early development. *Mol. Cell. Biol.* **24**, 2478-2486.

Ecco, G., Cassano, M., Kauzlaric, A., Duc, J., Coluccio, A., Offner, S., Imbeault, M., Rowe, H. M., Turelli, P. and Trono, D. (2016). Transposable elements and their KRAB-ZFP controllers regulate gene expression in adult tissues. *Dev. Cell* **36**, 611-623.

Fadloun, A., Le Gras, S., Jost, B., Ziegler-Birling, C., Takahashi, H., Gorab, E., Carninci, P. and Torres-Padilla, M.-E. (2013). Chromatin signatures and retrotransposon profiling in mouse embryos reveal regulation of LINE-1 by RNA. *Nat. Struct. Mol. Biol.* **20**, 332-338.

Fei, Q., Shang, K., Zhang, J., Chuai, S., Kong, D., Zhou, T., Fu, S., Liang, Y., Li, C., Chen, Z. et al. (2015). Histone methyltransferase SETDB1 regulates liver cancer cell growth through methylation of p53. *Nat. Commun.* **6**, 8651.

Grieco, D., Porcellini, A., Avvedimento, E. V. and Gottesman, M. E. (1996). Requirement for cAMP-PKA pathway activation by M phase-promoting factor in the transition from mitosis to interphase. *Science* **271**, 1718-1723.

Han, S. J. and Conti, M. (2006). New pathways from PKA to the Cdc2/cyclin B complex in oocytes: Wee1B as a potential PKA substrate. *Cell Cycle* **5**, 227-231.

Han, S. J., Chen, R., Paronetto, M. P. and Conti, M. (2005). Wee1B is an oocyte-specific kinase involved in the control of meiotic arrest in the mouse. *Curr. Biol.* **15**, 1670-1676.

Hao, Z., Zhang, H. and Cowell, J. (2012). Ubiquitin-conjugating enzyme UBE2C: molecular biology, role in tumorigenesis, and potential as a biomarker. *Tumour Biol.* **33**, 723-730.

Hatanaka, Y., Inoue, K., Oikawa, M., Kamimura, S., Ogonuki, N., Kodama, E. N., Ohkawa, Y., Tsukada, Y. and Ogura, A. (2015). Histone chaperone CAF-1 mediates repressive histone modifications to protect preimplantation mouse embryos from endogenous retrotransposons. *Proc. Natl. Acad. Sci. USA* **112**, 14641-14646.

Hirao, Y., Miyano, T. and Kato, S. (1993). Acquisition of maturational competence in in vitro grown mouse oocytes. *J. Exp. Zool.* **267**, 543-547.

Hutnick, L. K., Huang, X., Loo, T.-C., Ma, Z. and Fan, G. (2010). Repression of retrotransposal elements in mouse embryonic stem cells is primarily mediated by a DNA methylation-independent mechanism. *J. Biol. Chem.* **285**, 21082-21091.

Inoue, A., Nakajima, R., Nagata, M. and Aoki, F. (2008). Contribution of the oocyte nucleus and cytoplasm to the determination of meiotic and developmental competence in mice. *Hum. Reprod.* **23**, 1377-1384.

Karess, R. (2005). Rod-Zw10-Zwilch: a key player in the spindle checkpoint. *Trends Cell Biol.* **15**, 386-392.

Karimi, M. M., Goyal, P., Maksakova, I. A., Bilenky, M., Leung, D., Tang, J. X., Shinkai, Y., Mager, D. L., Jones, S., Hirst, M. et al. (2011). DNA methylation and SETDB1/H3K9me3 regulate predominantly distinct sets of genes, retroelements, and chimeric transcripts in mESCs. *Cell Stem Cell* **8**, 676-687.

Kaustov, L., Ouyang, H., Amaya, M., Lemak, A., Nady, N., Duan, S., Wasney, G. A., Li, Z., Vedadi, M., Schapira, M. et al. (2011). Recognition and specificity determinants of the human cbx chromodomains. *J. Biol. Chem.* **286**, 521-529.

Kim, J., Zhao, H., Dan, J., Kim, S., Hardikar, S., Hollowell, D., Lin, K., Lu, Y., Takata, Y., Shen, J. et al. (2016). Maternal setdb1 is required for meiotic progression and preimplantation development in mouse. *PLoS Genet.* **12**, e1005970.

Kubiak, J. Z., Ciemerych, M. A., Hupalowska, A., Sikora-Polaczek, M. and Polanski, Z. (2008). On the transition from the meiotic to mitotic cell cycle during early mouse development. *Int. J. Dev. Biol.* **52**, 201-217.

Liu, H. and Aoki, F. (2002). Transcriptional activity associated with meiotic competence in fully grown mouse GV oocytes. *Zygote* **10**, 327-332.

Liu, C., Liu, Y., Wu, D., Luan, Z., Wang, E. and Yu, B. (2013). Ser 15 of WEE1B is a potential PKA phosphorylation target in G2/M transition in one-cell stage mouse embryos. *Mol. Med. Rep.* **7**, 1929-1937.

Liu, S., Brind'Amour, J., Karimi, M. M., Shirane, K., Bogutz, A., Lefebvre, L., Sasaki, H., Shinkai, Y. and Lorincz, M. C. (2014). Setdb1 is required for germline development and silencing of H3K9me3-marked endogenous retroviruses in primordial germ cells. *Genes Dev.* **28**, 2041-2055.

Lohmann, F., Loureiro, J., Su, H., Fang, Q., Lei, H., Lewis, T., Yang, Y., Labow, M., Li, E., Chen, T. et al. (2010). KMT1E mediated H3K9 methylation is required for the maintenance of embryonic stem cells by repressing trophectoderm differentiation. *Stem Cells* **28**, 201-212.

Loyola, A., Tagami, H., Bonaldi, T., Roche, D., Quivy, J. P., Imhof, A., Nakatani, Y., Dent, S. Y. R. and Almouzni, G. (2009). The HP1alpha-CAF1-SetDB1-containing complex provides H3K9me1 for Suv39-mediated K9me3 in pericentric heterochromatin. *EMBO Rep.* **10**, 769-775.

Madgwick, S., Hansen, D. V., Levasseur, M., Jackson, P. K. and Jones, K. T. (2006). Mouse Emi2 is required to enter meiosis II by reestablishing cyclin B1 during interkinesis. *J. Cell Biol.* **174**, 791-801.

Mall, M., Walter, T., Gorjánácz, M., Davidson, I. F., Nga Ly-Hartig, T. B., Ellenberg, J. and Mattaj, I. W. (2012). Mitotic lamin disassembly is triggered by lipid-mediated signaling. *J. Cell Biol.* **198**, 981-990.

Masciarelli, S., Horner, K., Liu, C., Park, S. H., Hinckley, M., Hockman, S., Nedachi, T., Jin, C., Conti, M. and Manganiello, V. (2004). Cyclic nucleotide phosphodiesterase 3A-deficient mice as a model of female infertility. *J. Clin. Invest.* **114**, 196-205.

Matsui, T., Leung, D., Miyashita, H., Maksakova, I. A., Miyachi, H., Kimura, H., Tachibana, M., Lorincz, M. C. and Shinkai, Y. (2010). Proviral silencing in embryonic stem cells requires the histone methyltransferase ESET. *Nature* **464**, 927-931.

Moore, G. P. M., Lintern-Moore, S., Peters, H. and Faber, M. (1974). RNA synthesis in the mouse oocyte. *J. Cell Biol.* **60**, 416-422.

Nestorov, P., Tardat, M. and Peters, A. H. F. M. (2013). H3K9/HP1 and Polycomb: two key epigenetic silencing pathways for gene regulation and embryo development. *Curr. Top. Dev. Biol.* **104**, 243-291.

Norris, R. P., Ratzan, W. J., Freudzon, M., Mehlmann, L. M., Krall, J., Movsesian, M. A., Wang, H., Ke, H., Nikolaev, V. O. and Jaffe, L. A. (2009). Cyclic GMP from the surrounding somatic cells regulates cyclic AMP and meiosis in the mouse oocyte. *Development* **136**, 1869-1878.

Peaston, A. E., Evsikov, A. V., Graber, J. H., de Vries, W. N., Holbrook, A. E., Solter, D. and Knowles, B. B. (2004). Retrotransposons regulate host genes in mouse oocytes and preimplantation embryos. *Dev. Cell* **7**, 597-606.

Peters, A. H. F. M., O'Carroll, D., Scherthan, H., Mechtler, K., Sauer, S., Schöfer, C., Weipoltshammer, K., Pagani, M., Lachner, M., Kohlmaier, A. et al. (2001). Loss of the Suv39h histone methyltransferases impairs mammalian heterochromatin and genome stability. *Cell* **107**, 323-337.

Peters, A. H. F. M., Kubicek, S., Mechtler, K., O'Sullivan, R. J., Derijck, A. A. H. A., Perez-Burgos, L., Kohlmaier, A., Opravil, S., Tachibana, M., Shinkai, Y. et al. (2003). Partitioning and plasticity of repressive histone methylation states in mammalian chromatin. *Mol. Cell* **12**, 1577-1589.

Poueymirou, W. T. and Schultz, R. M. (1987). Differential effects of activators of cAMP-dependent protein kinase and protein kinase C on cleavage of one-cell

Development (2016) 143, 2767-2779 doi:10.1242/dev.132746

mouse embryos and protein synthesis and phosphorylation in one- and two-cell embryos. *Dev. Biol.* **121**, 489-498.

Puschendorf, M., Terranova, R., Boutsma, E., Mao, X., Isono, K.-i., Brykczynska, U., Kolb, C., Otte, A. P., Koseki, H., Orkin, S. H. et al. (2008). PRC1 and Suv39h specify parental asymmetry at constitutive heterochromatin in early mouse embryos. *Nat. Genet.* **40**, 411-420.

Ribet, D., Louvet-Vallee, S., Harper, F., de Parseval, N., Dewannieux, M., Heidmann, O., Pierron, G., Maro, B. and Heidmann, T. (2008). Murine endogenous retrovirus MuERV-L is the progenitor of the "orphan" epsilon viruslike particles of the early mouse embryo. *J. Virol.* **82**, 1622-1625.

Schindler, K., and Schultz, R. M. (2009). CDC14B acts through FZR1 (CDH1) to prevent meiotic maturation of mouse oocytes. *Biol. Reprod.* **80**, 795-803.

Schuh, M. and Ellenberg, J. (2007). Self-organization of MTOCs replaces centrosome function during acentrosomal spindle assembly in live mouse oocytes. *Cell* **130**, 484-498.

Schuh, M. and Ellenberg, J. (2008). A new model for asymmetric spindle positioning in mouse oocytes. *Curr. Biol.* **18**, 1986-1992.

Schultz, R. M., Montgomery, R. R. and Belanoff, J. R. (1983). Regulation of mouse oocyte meiotic maturation: implication of a decrease in oocyte cAMP and protein dephosphorylation in commitment to resume meiosis. *Dev. Biol.* **97**, 264-273.

Shi, Y., Desponts, C., Do, J. T., Hahm, H. S., Schöler, H. R. and Ding, S. (2008). Induction of pluripotent stem cells from mouse embryonic fibroblasts by Oct4 and Klf4 with small-molecule compounds. *Cell Stem Cell* **3**, 568-574.

Sommer, C., Strähle, C., Köthe, U. and Hamprecht, F. A. (2011). ilastik: Interactive Learning and Segmentation Toolkit. *Proceedings of the Eighth IEEE International Symposium on Biomedical Imaging*, 230-233.

Su, Y.-Q., Sugiura, K., Sun, F., Pendola, J. K., Cox, G. A., Handel, M. A., Schimenti, J. C. and Eppig, J. J. (2012). MARF1 regulates essential oogenic processes in mice. *Science* **335**, 1496-1499.

Sun, Q.-Y., Miao, Y.-L. and Schatten, H. (2009). Towards a new understanding on the regulation of mammalian oocyte meiosis resumption. *Cell Cycle* **8**, 2741-2747.

Svoboda, P., Stein, P., Anger, M., Bernstein, E., Hannon, G. J. and Schultz, R. M. (2004). RNAi and expression of retrotransposons MuERV-L and IAP in preimplantation mouse embryos. *Dev. Biol.* **269**, 276-285.

Tan, S.-L., Nishi, M., Ohtsuka, T., Matsui, T., Takemoto, K., Kamio-Miura, A., Aburatani, H., Shinkai, Y. and Kageyama, R. (2012). Essential roles of the histone methyltransferase ESET in the epigenetic control of neural progenitor cells during development. *Development* **139**, 3806-3816.

Vaccari, S., Weeks, J. L., Hsieh, M., II, Menniti, F. S. and Conti, M. (2009). Cyclic GMP signaling is involved in the luteinizing hormone-dependent meiotic maturation of mouse oocytes. *Biol. Reprod.* **81**, 595-604.

van der Heijden, G. W., Derijck, A. A. H. A., Pósfai, E., Giele, M., Pelczar, P., Ramos, L., Wansink, D. G., van der Vlag, J., Peters, A. H. F. M. and de Boer, P. (2007). Chromosome-wide nucleosome replacement and H3.3 incorporation during mammalian meiotic sex chromosome inactivation. *Nat. Genet.* **39**, 251-258.

Van Duyne, R., Easley, R., Wu, W., Berro, R., Pedati, C., Klase, Z., Kehn-Hall, K., Flynn, E. K., Symer, D. E. and Kashanchi, F. (2008). Lysine methylation of HIV-1 Tat regulates transcriptional activity of the viral LTR. *Retrovirology* **5**, 40.

Veselovska, L., Smallwood, S. A., Saadeh, H., Stewart, K. R., Krueger, F., Maupetit-Méhouas, S., Arnaud, P., Tomizawa, S.-I, Andrews, S. and Kelsey, G. (2015). Deep sequencing and de novo assembly of the mouse oocyte transcriptome define the contribution of transcription to the DNA methylation landscape. *Genome Biol.* **16**, 209.

Walsh, C. P., Chaillet, J. R. and Bestor, T. H. (1998). Transcription of IAP endogenous retroviruses is constrained by cytosine methylation. *Nat. Genet.* **20**, 116-117.

Wang, H., An, W., Cao, R., Xia, L., Erdjument-Bromage, H., Chatton, B., Tempst, P., Roeder, R. G. and Zhang, Y. (2003). mAM facilitates conversion by ESET of dimethyl to trimethyl lysine 9 of histone H3 to cause transcriptional repression. *Mol. Cell* **12**, 475-487.

Watanabe, Y. (2012). Geometry and force behind kinetochore orientation: lessons from meiosis. *Nat. Rev. Mol. Cell Biol.* **13**, 370-382.

Wickramasinghe, D., Ebert, K. M. and Albertini, D. F. (1991). Meiotic competence acquisition is associated with the appearance of M-phase characteristics in growing mouse oocytes. *Dev. Biol.* **143**, 162-172.

Xie, C., Powell, C., Yao, M., Wu, J. and Dong, Q. (2014). Ubiquitin-conjugating enzyme E2C: a potential cancer biomarker. *Int. J. Biochem. Cell Biol.* **47**, 113-117.

Yeap, L.-S., Hayashi, K. and Surani, M. A. (2009). ERG-associated protein with SET domain (ESET)-Oct4 interaction regulates pluripotency and represses the trophectoderm lineage. *Epigenetics Chromatin* **2**, 12.

Yoshida, N. and Perry, A. C. (2007). Piezo-actuated mouse intracytoplasmic sperm injection (ICSI). *Nat. Protoc.* **2**, 296-304.

Yu, A., Zhang, Z., Bi, Q., Sun, B., Su, W., Guan, Y., Mu, R., Miao, C., Zhang, J. and Yu, B. (2008). Regulation of cAMP on the first mitotic cell cycle of mouse embryos. *Mol. Reprod. Dev.* **75**, 489-495.

Yuan, P., Han, J., Guo, G., Orlov, Y. L., Huss, M., Loh, Y.-H., Yaw, L.-P., Robson, P., Lim, B. and Ng, H.-H. (2009). Eset partners with Oct4 to restrict extraembryonic trophoblast lineage potential in embryonic stem cells. *Genes Dev.* **23**, 2507-2520.

Zuccotti, M., Ponce, R. H., Boiani, M., Guizzardi, S., Govoni, P., Scandroglio, R., Garagna, S. and Redi, C. A. (2002). The analysis of chromatin organisation allows selection of mouse antral oocytes competent for development to blastocyst. *Zygote* **10**, 73-78.

Zuccotti, M., Merico, V., Cecconi, S., Redi, C. A. and Garagna, S. (2011). What does it take to make a developmentally competent mammalian egg? *Hum. Reprod. Update* **17**, 525-540.

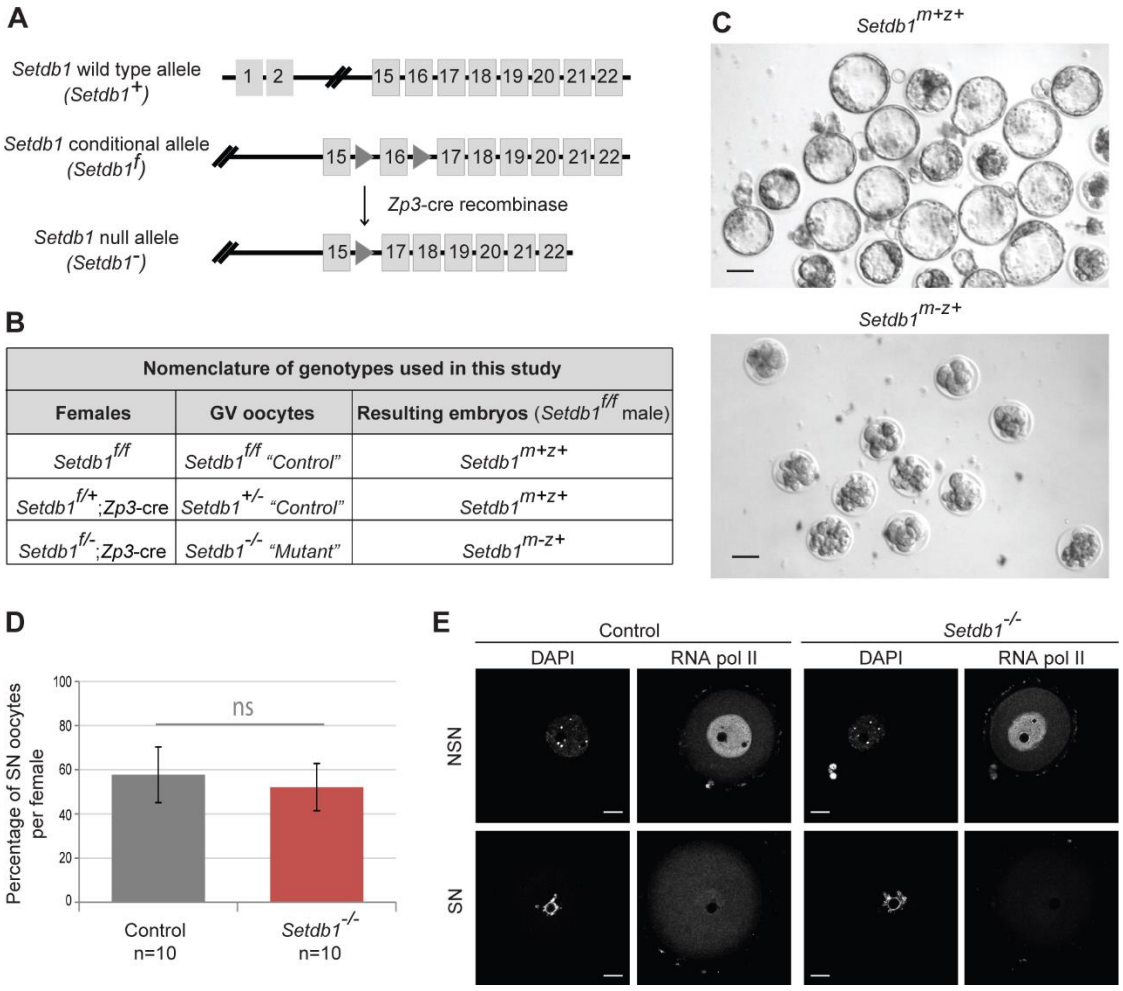

Figure S1 (related to Figure 1)

(A) Generation of *Setdb1*$^{f/f}$ mice (based on (Lohmann et al., 2010)). LoxP sites are represented as triangles. Excision of exon 16 by *ZP3*-cre mediated recombination between LoxP sites produces the *Setdb1* null allele. **(B)** Nomenclature of genotypes used in the study. **(C)** Differential interference contrast (DIC) images of E4.5 *Setdb1*$^{m+z+}$ and *Setdb1*$^{m-z+}$ *in vitro* cultured embryos. Scale bars: 50µm. **(D)** Percentage of SN-GV oocytes per female. n: number of mice analyzed. P-value was calculated using an unpaired t-test assuming equal variance; ns: non-significant. **(E)** RNA polymerase II (RNA pol II) staining on NSN and SN GV oocytes. At least 7 oocytes were analyzed for each condition. Scale bars: 20µm.

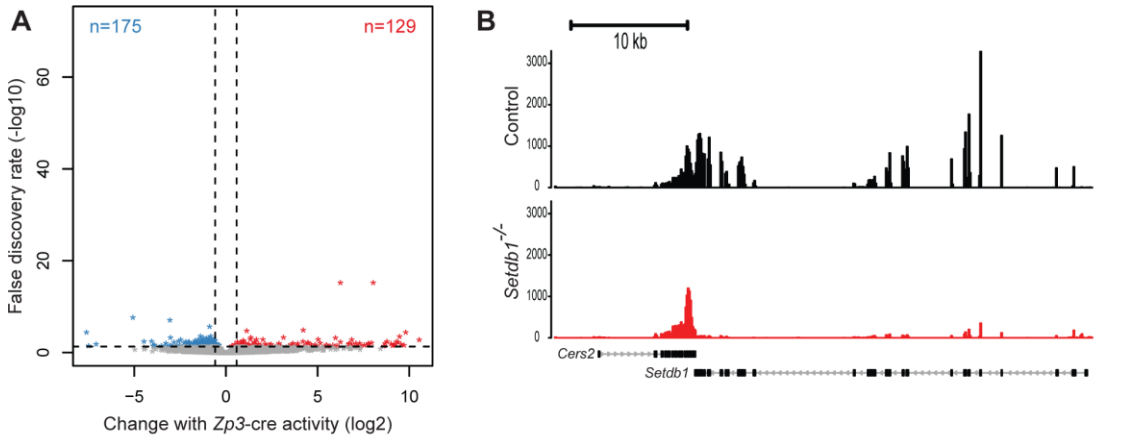

C

Cluster	Enrichment score	Processes	Count	P-Value
1	2.62	cell division	28	3.20E-05
		cell cycle	44	3.30E-04
		M phase	24	1.30E-03
		cell cycle phase	25	4.10E-03
		nuclear division	17	4.80E-03
		mitosis	17	4.80E-03
		cell cycle process	28	5.60E-03
		M phase of mitotic cell cycle	17	5.80E-03
		organelle fission	17	6.70E-03
		mitotic cell cycle	18	2.20E-02
2	2.1	cytoskeleton organization	25	3.80E-03
		actin filament-based process	16	5.50E-03
		actin cytoskeleton organization	15	7.50E-03
		actin filament organization	7	2.60E-02
3	2.03	phosphorylation	44	7.10E-03
		protein amino acid phosphorylation	40	7.70E-03
		phosphate metabolic process	50	1.20E-02
		phosphorus metabolic process	50	1.20E-02
4	1.83	blood vessel development	19	1.10E-02
		vasculature development	19	1.40E-02
		blood vessel morphogenesis	16	1.50E-02
		angiogenesis	12	2.00E-02

Cluster	Enrichment score	Processes	Count	P-Value
5	1.78	neural tube development	10	6.50E-03
		embryonic morphogenesis	25	1.20E-02
		chordate embryonic development	28	1.30E-02
		embryonic development endind in birth or egg hatching	28	1.50E-02
		in utero embryonic development	17	7.90E-02
6	1.69	cell projection organization	26	1.30E-03
		cell part morphogenesis	18	6.00E-03
		cell morphogenesis	23	7.90E-03
		cell projection morphogenesis	17	8.50E-03
		cellular component morphogenesis	25	9.20E-03
		cell motion	25	1.50E-02
		neuron development	21	1.60E-02
		neuron projection development	17	1.70E-02
		neuron differentiation	25	3.70E-02
		cell morphogenesis involved in differentiation	15	5.10E-02
		neuron projection morphogenesis	13	5.60E-02
		axonogenesis	12	6.90E-02
		axon guidance	8	1.00E-01
		cell morphogenesis involved in neuron differentiation	12	1.20E-01

Figure S2 (related to Figure 4)

(A) Volcano plot showing differentially expressed genes comparing *Setdb1*$^{f/+}$; *Zp3*-cre versus *Setdb1*$^{f/-}$ GV-oocytes, FDR<0.05. Blue: down-regulated genes; red: up-regulated genes. **(B)** Genome browser view of *Setdb1* locus. **(C)** Clustering of GO-terms. Count: number of genes in the cluster.

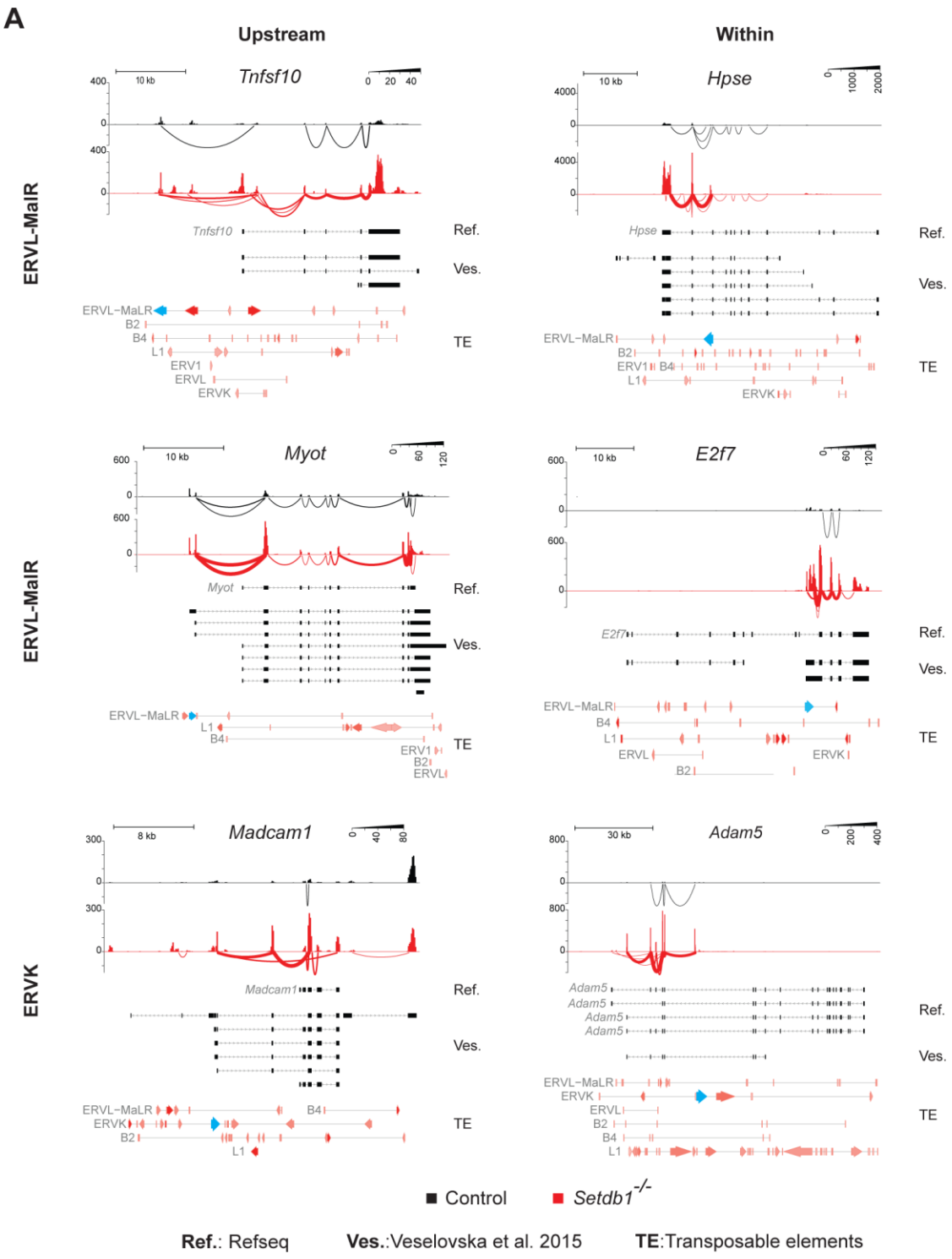

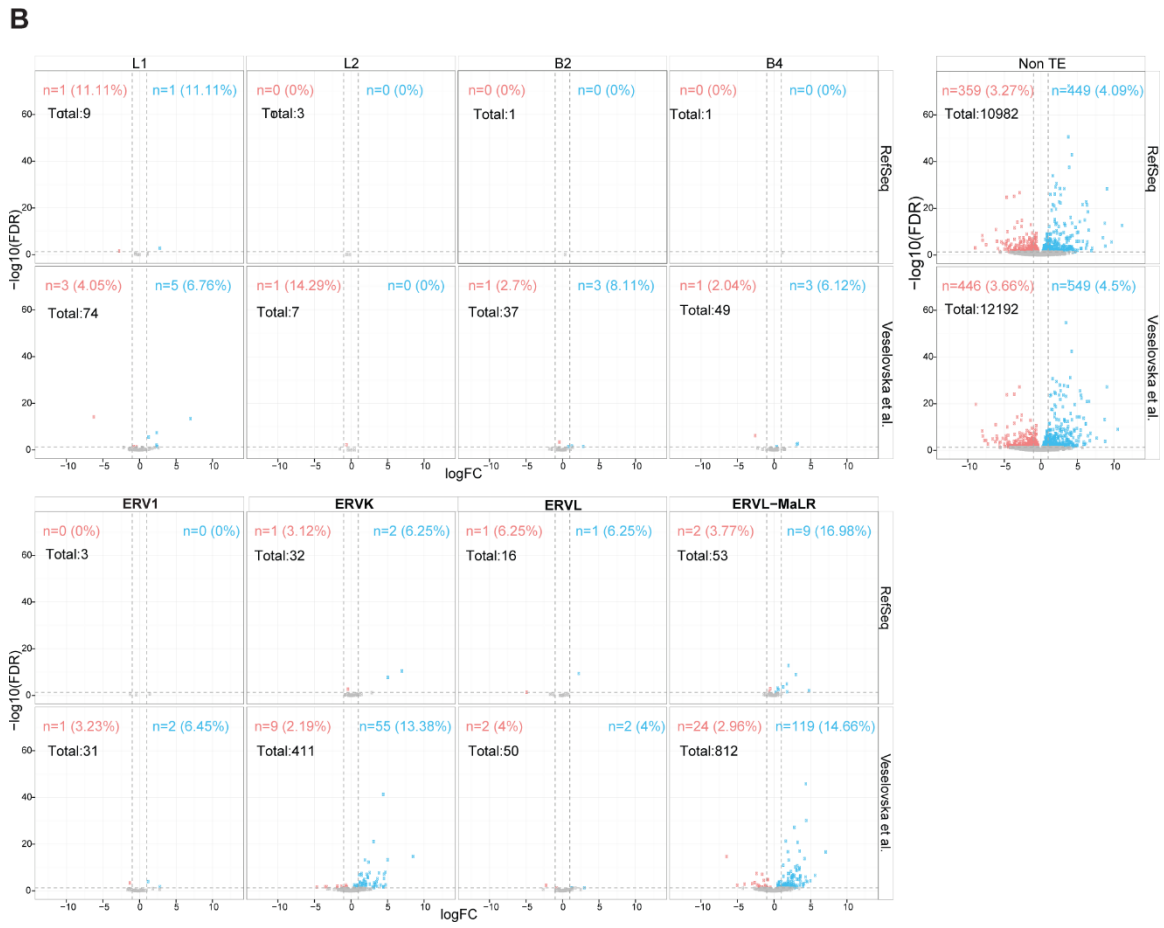

Figure S3 (related to Figure 5)

(A) Genome browser views illustrating expression along *Tnfsf10, Myot, Hpse, E2f7, Madcam1 and Adam5* loci (uniquely mapped reads per 100 base pair bins, library-size normalized) and expression at splice-junctions (uniquely mapped reads per splice-junction, library-size normalized) between ERVL-MaLR or ERVK elements and exons in control and *Setdb1*$^{-/-}$ oocytes. Splicing events occurred either with ERVs positioned upstream of or within the ORF (colored in blue), resulting in formation of chimaeric transcripts encoding for intact or likely aberrant proteins, respectively. **(B)** Volcano plots for multi-exonic transcripts with transcriptional start sites in different families of ERVs, using genome annotations based on RefSeq (top) and Veselovska et al. (Veselovska et al., 2015) (bottom).

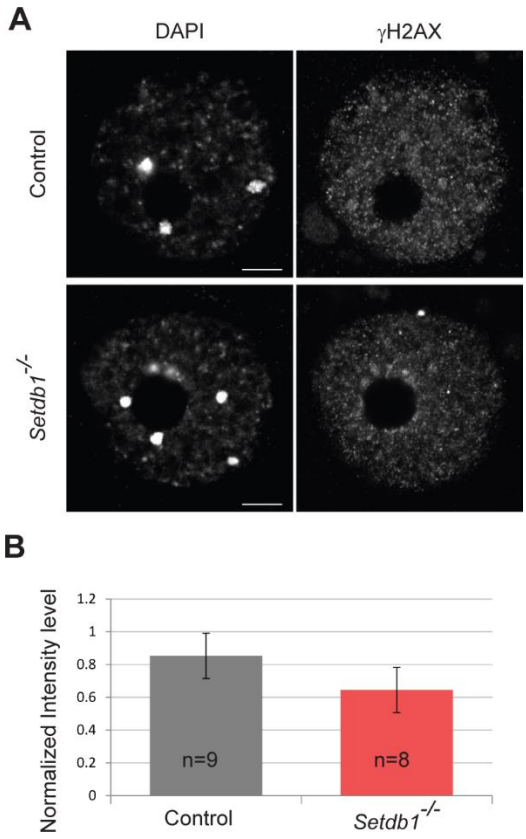

Figure S4

(A) γH2AX and DAPI staining on control and *Setdb1*$^{-/-}$ GV-oocytes. Scale bars: 20μm. **(B)** Three dimensional quantification of γH2AX levels in oocytes, normalized to nucleosomal staining. n:number of oocytes analyzed.

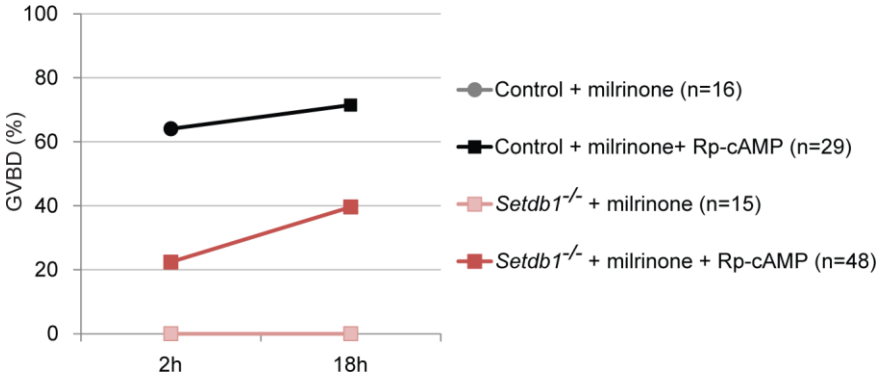

Figure S5 (related to Figure 6)

GVBD 2h and 18h after addition or in absence of Rp-cAMP in presence of milrinone.
n: number of oocytes analyzed.

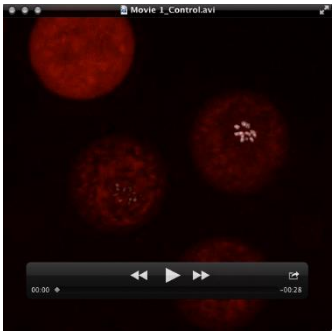

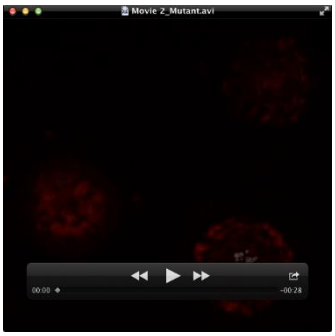

Movies 1 and 2 - related to Figure 2.

GV-oocytes were micro-injected with mRNA transcripts encoding for H2B-mCherry (grey) and α-tubulin (red). Meiotic maturation was followed by live-imaging using a spinning disc confocal microscope, at 37˚C degree with a 5% CO_2 environment. Oocytes were imaged every 15 minutes.

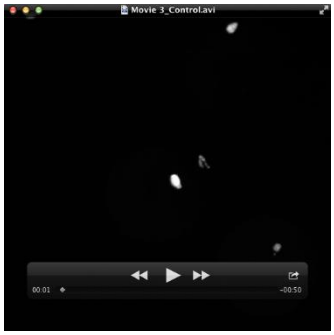

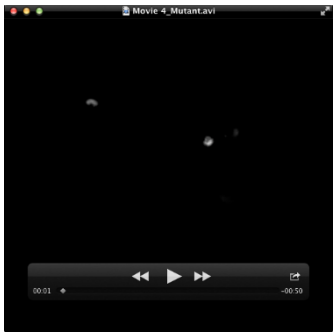

Movies 3 and 4 - related to Figure 7.

MII-oocytes were micro-injected with mRNA transcripts encoding for H2B-mCherry (grey) followed by intra cytoplasmic sperm injection. First cleavage was followed by live-imaging using a spinning disc confocal microscope, at 37˚C degree with a 5% CO_2 environment. Embryos were imaged every 15 minutes.

Table S1 – related to Figures 4 and 5

Differential expression data of genes and splice-junctions based on RefSeq annotation. The table allows a comparison of expression of splice-junctions to chimaeric transcripts identified by Peaston et al. (Peaston et al., 2004). The table provides also the names of genes present in GO-term gene clusters (see Fig. S2C).

Click here to Download Table S1

Table S2 – related to Figure 5.

Differential expression data of ERVs grouped according to repFamily annotation (RepBase).

Click here to Download Table S2

Table S3 – related to Figure 5.

Differential expression data of ERVs grouped according to repName annotation (RepBase).

Click here to Download Table S3

Table S4 – related to Figure 5.

Numbers of splice-junctions between different types of ERVs and exons in control and *Setdb1* mutant oocytes.

Click here to Download Table S4

Table S5 – related to Figure 5.

Differential expression data of transcripts and ERVs based on Veselovska et al. (Veselovska et al., 2015) annotation. The table provides a match between data based on the Veselovska and RefSeq annotations. The table provides also the names of genes present in GO-term gene clusters (see Fig. S2C).

Click here to Download Table S5

Supplementary methods

RNA sequencing. We performed expression profiling on pools of 16 denuded GV-oocytes isolated per mouse. We used oocytes from 4 *Setdb1*$^{f/+}$*; Zp3*-cre mice and 2 *Setdb1*$^{f/-}$ mice as controls and oocytes from 4 *Setdb1*$^{f/-}$; *Zp3*-cre mice as mutant. RNA was isolated using the RNeasy Micro Kit (Qiagen). cDNA was generated and amplified from 1.2ng with the NuGen ovation RNA-seq System V2 (Part no. 7102; NuGen). 50ng of the resulting SPIA cDNA was fragmented and sequencing libraries were prepared using TruSeq DNA Sample Preparation Kit (low-throughput protocol) (Part no. 15005180 Rev. C; NuGen). Libraries were pooled equimolarly and sequenced for 50 cycles on an Illumina HiSeq 2000 instrument using RTA 1.13.48 for basecalling. Demultiplexing and fastq generation was performed with bcl2fastq (bcl2fastq-1.8.3).

Read alignment and expression quantification. The *M. musculus* genome assembly (GRCm38/mm10 Dec. 2011), RepeatMasker repeat annotation (downloaded on 7 March 2012), RefSeq gene models (downloaded from UCSC on 4 February 2016), and the oocyte transcriptome annotation (downloaded on 29 February 2016 from the web page of the paper (Veselovska et al., 2015)) were used as a basis for all analyses. Illumina adaptor sequences (GATCGGAAGAGCACACGTCTGAACTCCAGTCAC) were removed from the 3' end of RNA sequencing reads and spliced alignment of reads to the genome was created using STAR of version 2.5.0a (Dobin et al., 2013) with parameters –outFilterMultimapNmax 300 –outMultimapperOrder Random -outSAMmultNmax 1 -outSAMmapqUnique 255 –alignSJoverhangMin 8, tracking up to 300 matches and choosing only one random match for reads with multiple alignments, gapped alignments with overhang shorter than 8 bp were removed.

For quantification of mRNA uniquely aligned reads were summed per transcripts using QuasR package (version 1.10.1) (Gaidatzis et al., 2015) and for genes with multiple transcripts, the transcript with the maximal average expression over all samples was selected as the representative.

For quantification of expression of repetitive elements all reads, including multimappers, were summed per repeat names or per repeat families. For Fig. 5E only uniquely mapped reads were used (here corresponding to reads with minimum mapping quality 255).

For display in heatmaps, RPKM values were calculated (Mortazavi et al., 2008) (and log2 transformed using formula log2(RPKM + psc) – log2(psc) where pseudo-count psc was set to 0.1. Comparison between RefSeq transcriptome annotation and oocyte transcriptiome annotation was done using *cuffcompare* from Cufflinks suite (Trapnell et al., 2012).

Differential expression analysis. Differentially expressed genes and repeat elements were identified using R and edgeR version 3.12.0 (McCarthy et al., 2012), by fitting a two-factor model of the form “cre + genotype”, with cre corresponding to expression status of the *Zp3* cre-recombinase (“expressed” or “not expressed”), and genotype to the *Setdb1* genotype (“+/-“ or “-/-“). The cre factor was included into the model to absorb the effects of expressing *Zp3*-cre, independent of the genotype of Setdb1. Only genes with at least 3 reads per million in at least two samples were included in the analysis (11,366 for RefSeq annotation and 14,954 for oocyte specific annotation). P-values for differential expression were calculated using log-likelihood tests. Differentially expressed genes or repeat elements were defined by FDR<0.05. For Fig. S3B, RefSeq transcripts and oocyte transcripts from Veselovska et al. (2015) were classified as being initiated from a transposable element (TE) if the 5’ end of the transcript overlapped with the TE on the same strand. GO term analysis and clustering were performed using DAVID (Huang da et al., 2009a, b).

Analysis of splicing events. SJ.out.tab files produced by STAR for each sample were loaded into R environment and combined into a matrix containing the number of reads supporting each observed splicing event in each sample. Splicing events which were not supported by at least 5 reads in at least 2 samples and very long splicing events (longer than half of the average transcript length, ~47 Kbp) were removed from the analysis. Differential expression analysis was carried out similarly to the analysis for genes and repeats. Splicing events were classified “Upstream” with respect to a RefSeq transcript if the intron started upstream of the TSS and ended within the transcript. Splicing events were classified as “Within” if both intron start and end were within a transcript, and as “Downstream” if the intron started within and ended downstream of the transcript. Splicing events were classified as TE-associated if intron starts overlapped TE on any strand.

Supplementary references

Dobin, A., Davis, C.A., Schlesinger, F., Drenkow, J., Zaleski, C., Jha, S., Batut, P., Chaisson, M., and Gingeras, T.R. (2013). STAR: ultrafast universal RNA-seq aligner. Bioinformatics. *29(1)*, 15-21.

Gaidatzis, D., Lerch, A., Hahne, F., and Stadler, M.B. (2015). QuasR: quantification and annotation of short reads in R. Bioinformatics *31(7)*, 1130-1132.

Huang da, W., Sherman, B.T., and Lempicki, R.A. (2009a). Bioinformatics enrichment tools: paths toward the comprehensive functional analysis of large gene lists. Nucleic Acids Res *37*, 1-13.

Huang da, W., Sherman, B.T., and Lempicki, R.A. (2009b). Systematic and integrative analysis of large gene lists using DAVID bioinformatics resources. Nat Protoc *4*, 44-57.

McCarthy, D.J., Chen, Y., and Smyth, G.K. (2012). Differential expression analysis of multifactor RNA-Seq experiments with respect to biological variation. Nucleic Acids Res *40*, 4288-4297.

Mortazavi, A., Williams, B.A., McCue, K., Schaeffer, L., and Wold, B. (2008). Mapping and quantifying mammalian transcriptomes by RNA-Seq. Nat Methods *5*, 621-628.

Peaston, A.E., Evsikov, A.V., Graber, J.H., de Vries, W.N., Holbrook, A.E., Solter, D., and Knowles, B.B. (2004). Retrotransposons regulate host genes in mouse oocytes and preimplantation embryos. Developmental cell *7*, 597-606.

Veselovska, L., Smallwood, S.A., Saadeh, H., Stewart, K.R., Krueger, F., Maupetit-Mehouas, S., Arnaud, P., Tomizawa, S., Andrews, S., and Kelsey, G. (2015). Deep sequencing and de novo assembly of the mouse oocyte transcriptome define the contribution of transcription to the DNA methylation landscape. Genome biology *16*, 209.